

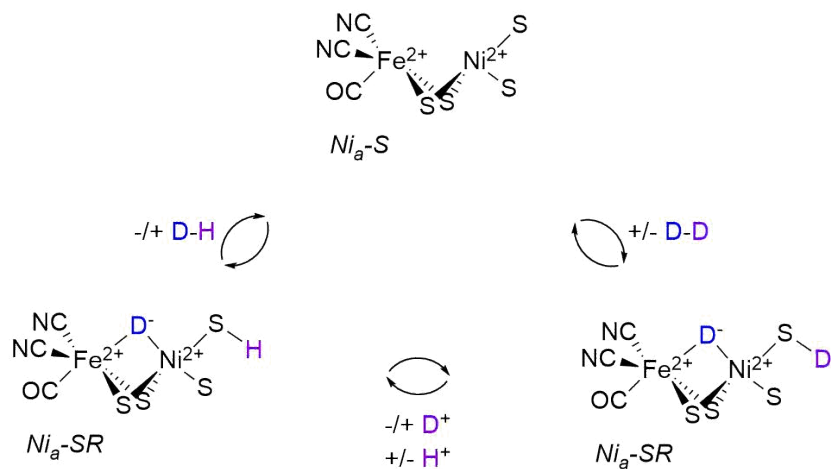
Supplementary Information for
Metal-Ligand Cooperativity in the Soluble Hydrogenase-1 from *Pyrococcus Furiosus*

Gregory E. Vansuch, Chang-Hao Wu, Dominik K. Haja, Shoshawn A. Blair, Bryant Chica, Michael K. Johnson, Michael W.W. Adams, and R. Brian Dyer

Contents

Scheme S2: General [NiFe]-Hydrogenase H/D Exchange Mechanism.....	2
Experimental Details.....	3 – 5
1. General Considerations	
2. Protein Preparation and Purification	
3. CdSe /CdS Dot-in Rod Preparation	
4. Proton Reduction and Hydrogen Oxidation Activity	
5. H/D Exchange	
6. Electron Paramagnetic Resonance Spectroscopy	
7. Steady State Photochemical Reduction with Fourier Transform Infrared Spectroscopy of R355K SH1	
8. pH Dependent FTIR Spectroscopy of R355K <i>Pf</i> SH1	
9. FTIR Spectroscopy of CO Inhibited Native, E17Q, and R355K <i>Pf</i> SH1	
10. Methyl Viologen Oxidation Reduction of Native and R355K <i>Pf</i> SH1 Under 5% H ₂ Monitored via UV-Vis Spectroscopy	
Data Analysis	
1. H/D Exchange.....	6 – 12
• <i>Figures S1 – S5</i>	
• <i>Table S1 – S2</i>	
2. Electron Paramagnetic Resonance Spectroscopy.....	13 – 19
• <i>Figures S6 – S9</i>	
• <i>Tables S3 – S8</i>	
3. Fourier Transform Infrared Spectroscopy, Equilibrium Photochemical Reduction.....	20 – 22
• <i>Figures S10 – S12</i>	
4. Fourier Transform Infrared Spectroscopy pH Dependence and Temperature Dependence Sample.....	23 – 38
• <i>pH dependent infrared spectra</i>	
○ <i>Figures S13 – S20, Table S9</i>	25 – 32
○ <i>Tables S9– S12</i>	33
• <i>Temperature Dependent spectra of pH = 8.5 Sample, Figure S21</i>	34
• <i>Slow oxidation spectra of pH = 9.3 sample</i>	35 – 37
○ <i>Figures S22 – S23</i>	
○ <i>Tables S13 – S14</i>	
5. Fourier Transform Infrared Spectroscopy Samples Incubated Under a CO Atmosphere.....	38 – 42
• <i>Figures S24 – S27</i>	
• <i>Tables S15 – S16</i>	
6. Temperature Methyl Viologen Oxidation Reduction of Native and R355K <i>Pf</i> SH1 Under 5% H ₂ Monitored via UV-Vis Spectroscopy.....	43 – 44
7. Additional Analysis: pK _a of K355 in Ni ₃ ³⁺ -C Likely not Perturbed from Solution Value.....	45
8. Additional Analysis of the CN Features and Exogenous CO Binding Results Features.....	45– 46
• <i>Tables S17 – S18</i>	
Supplemental Information References.....	47 – 48

Scheme S1: General H/D Exchange Mechanism for [NiFe]-Hydrogenases



Experimental

1. General Considerations

All infrared and UV-Vis sample preparations were carried out in an anaerobic glove box or glove bag (Coy Laboratory Products, Inc.) containing a ~ 4% +/- 1% hydrogen and ~ 95% nitrogen atmosphere, with only gas exchange occurring outside the glove box or bag (e.g. CO incubation). The EPR sample preparations were carried out in an anaerobic glove bag (Coy Laboratory Products, Inc.) containing an ~ 3% +/- 1% hydrogen and ~ 97% argon gas mix. All purchased chemicals were used as received. Buffers were purged with the glove box or glove bag atmosphere prior to use for at least 30 – 40 minutes. Synthetic procedures were carried out using standard Schlenk techniques.

2. Protein Preparation and Purification

Native soluble hydrogenase-1 from *Pyrococcus furiosus* (Pf SH1) was expressed and purified as described previously.¹ The plasmid encoding the R355K and E17Q variant was prepared using the QuikChange Site-Directed Mutagenesis Kit (Agilent Technologies) as described previously.² The site directed mutated gene was amplified from the sequence confirmed plasmid and assembled with the *pyrF* selection marker, P_{slp} as the promoter, a 9x-His tag at the N-terminus, and upstream (UFR) and downstream (DFR) flanking regions by overlapping PCR as previously reported.¹ The flanking regions were targeted to the intergenic space between PF0574 and PF0575. By homologous recombination, the linear knock-in cassette was transformed into MW0015 ($\Delta pyrF \Delta sh1\beta\gamma\delta\alpha \Delta sh11\beta\gamma\delta\alpha$), which does not contain any cytoplasmic hydrogenase activity. The sequence-confirmed clone (MW0530) was used for large scale fermentation, protein purification, and characterization.³ Briefly, cells were harvested from a 20L fermenter and lysed in 25 mM sodium phosphate, pH 7.5, containing 1 mM dithiothreitol (DTT) and 50 $\mu\text{g}/\text{mL}$ DNase I with a cell to buffer ratio of 1:5 (g, wet weight : mL) in an anaerobic chamber. The cytoplasmic fraction obtained after ultracentrifugation was directly loaded on a Ni-NTA column and the bound protein was obtained by gradient elution. The hydrogenase was further purified by QFF chromatography and used for subsequent activity assays and spectroscopic characterization discussed herein. The purified enzyme was stored in 50 mM phosphate buffer containing 2 mM DTT and 300 mM NaCl (pH = 8.0) in an anaerobic atmosphere (~4% H₂ and 96% nitrogen or argon atmosphere). These storage conditions allow for standard EPR and FTIR sample preparations to exhibit activated forms of the enzyme at the Ni_a²⁺-S level and further reduced states.

3. CdSe/CdS Dot-in Rod and propyl-bridged 2-2'-bipyridinium (PDQ) Preparation

50 nm CdSe/CdS dot-in-rod nanostructures were synthesized and exchanged with mercaptopropionic acid ligands as previously described.^{4,5}

PDQ was synthesized based on reported procedure with minor modifications.^{5,6} Briefly, 6 g of 2,2'-bipyridine was heated to 100 °C in 20 mL of 1,3-dibromo propane for 2-3 hours. The resultant solid product was filtered and (re)crystallized from methanol x 2. Purity was verified by NMR.

4. Proton Reduction and Hydrogen Oxidation Activity

Proton reduction activity and hydrogen oxidation activity of native, E17Q, and R355K PfSH1 were measured using a previously reported method.² Briefly, hydrogen production assays utilized 8 ml glass vials containing 2 ml of 100 mM anaerobic HEPPS buffer (pH = 8.4; this pH value ensures maximum reduction potential of dithionite for increased reducing conditions and also maximum methyl viologen radical formation⁷) containing 10 mM dithionite as the electron donor and 1 mM methyl viologen as the electron mediator. The sample vials were incubated at 80 °C for 1 minute and the assay was initiated by the addition of the enzyme. The amount of hydrogen in the headspace was monitored for 6 minutes using a 6580 Network Gas Chromatography (GC) system from Agilent Technologies. Hydrogen oxidation activity was measured by incubating the enzyme in hydrogen-saturated 100 mM EPPS buffer (pH = 8.4) in an anaerobic cuvette for ~ 5 minutes. The reaction was initiated by the addition of 1 mM benzyl viologen as the electron acceptor. The rate of hydrogen oxidation was determined by the rate of benzyl viologen reduction, which was monitored at 580 nm ($\epsilon \approx 8800 \text{ cm}^{-1} \text{ M}^{-1}$). The activities are reported as specific activity, U/mg, where 1 U = μmol of H₂ produced or oxidized min⁻¹.

5. H/D Exchange*

Samples of native SH1 were prepared by diluting an enzyme stock to 222 nM in a quartz cuvette (1 cm x 1 cm) in pH = 6.3, 50 mM potassium phosphate buffer. A stock dithionite was then added to the cuvette (working concentration of 1.5 mM). The cuvette was sealed with a rubber stopper and Teflon tape, and the headspace was then purged with D₂ gas (99.8 % atom D, Sigma Aldrich) for ~ 15 minutes while the solution was vigorously stirred with a magnetic stir bar. The R355K sample preparation was identical except the enzyme concentration was 412 nM and the cuvette was purged with D₂ gas for 70 minutes because we had previously observed larger incubation times are required for optimal activity with SH1 variants.

A given sample was then placed in the path of a continuous 532 nm excitation beam from a Verdi laser (Coherent, Inc) operating at 0.9 W. The Raman scatter was collected as described previously with minor modifications.⁸ Briefly, scatter was focused, collimated, and sent to a 0.275 m focal length spectrograph (Acton Research Corporation). The spectrograph grating was set to disperse the region of the Q1 branches of D₂, HD, and H₂ (~ 3000 – 4000 cm⁻¹⁹) onto a CCD Camera (Acton/Princeton Research Corporation) operating at - 75 °C. Data were collected using a home-built LabView program. The camera exposure time was set to 4 minutes per data point. The solution was stirred with a magnetic stir bar to ensure transfer of HD into the headspace and continual transfer of D₂ to solution. Native SH1 data were collected for 800 minutes and R355K data were collected for 1200 minutes.

Standards of H₂ (Nexair), D₂ (99.8% atom D; Sigma Aldrich), and HD (96 % mol HD, 98% atom D; Sigma Aldrich) for calibration were measured using an identical camera exposure time in an otherwise empty cuvette with the Verdi operating at 0.85 W.

**It is appropriate to note that, independent of prior work in our laboratory¹⁰ and what is reported in this manuscript, Kawahara-Nakagawa and co-workers developed a similar methodology for measuring H/D exchange with hydrogenases that was recently published.¹¹*

6. Electron Paramagnetic Resonance Spectroscopy

A stock of native or R355K enzyme was exchanged x 5 into 25 mM MOPS (pH = 6.7) or 25 mM glycine (pH = 9.3) in an ~3% hydrogen, 97% argon atmosphere. The final volumes were adjusted to 250 µL which resulted in enzyme concentrations of ~ 0.13 mM for native SH1 and 0.80 mM for R355K SH1. Samples were transferred to EPR tubes and flash frozen in liquid N₂. Low temperature EPR spectra were recorded using an EMXplus spectrometer and an ER4112HV-11 cryostat mated to a cryogen-free Stinger F70L closed cycle refrigeration system (Bruker BioSpin). The temperature was 70 K except for the pH = 6.7 R355K sample that was run at 50 K (we were unable to observe signals at 70 K). The modulation frequency was 100 kHz, the modulation amplitude was 0.4 mT, and the microwave power was 10 mW. For native SH1, 100 scans were averaged at pH = 6.7, and 500 scans were averaged at pH = 9.3. For R355K SH1, 225 scans were averaged at pH = 6.7, and 100 scans were averaged at pH = 9.3.

7. Steady State Photochemical Reduction Coupled to Fourier Transform Infrared Spectroscopy with R355K SH1

All FTIR samples were prepared in a manner similar to those reported for native¹² and E17Q² P_fSH1 with minor modifications for the equilibrium photochemical reduction.⁴

4.8 mg of R355K SH1 stock was exchanged x 5 into an Amicon 50 kDa filter (Millipore) for at least 8 minutes in 30 mM potassium phosphate/50 mM MPA, pH = 7.23 buffer. MPA is the sacrificial electron donor. In a separate 50 kDa filter, CdSe/CdS dot-in-rods were exchanged into the same buffer and brought to a final volume such that the *total* sample volume would result in an OD of the rods being ~ 0.15 - 0.3. The R355K and dot-in-rods were then transferred to a low volume vial (Verex™). Afterwards, a PDQ stock was gently mixed into the solution; this brought the total solution volume to ~15 µL, resulting in an enzyme concentration of ~ 2 mM (assuming a molecular weight of 153 kDa) and a PDQ²⁺ concentration of 30 mM. A reference solution was prepared identically with a working concentration of 1.73 mM metmyoglobin. The sample and reference were then loaded into a copper plated IR cell between two CaF₂ windows that were vertically split by a Teflon spacer (path length = 76.2 µm) via injection through small port holes with a gas tight syringe. The ports were then sealed to ensure the sample remained anaerobic.

The copper cell was then placed in a dry air purged, home built-external beam compartment of a Varian 660 Fourier Transform Infrared (FTIR) spectrometer equipped with a translation stage and a liquid nitrogen cooled MCT detector (Kolmar, Inc.). Prior to initiation of the photochemical reduction, 4096 scans of the sample and reference were obtained with a 2 cm⁻¹ resolution at lab temperature (~ 20 +/- 1 °C). The sample was then illuminated for periods of 1 – 20 min with a 405 nm laser diode (~ 4 mW, Thor Labs, Inc.). The beam was defocused by a plano-concave lens to allow for uniform illumination of the sample. Following each illumination time, the sample was allowed to equilibrate to the new reducing conditions and then 4096 scans of the sample were obtained.

8. pH Dependent FTIR Samples of R355K SH1

To prepare samples for pH dependent FTIR spectroscopy, 1 – 2 mL of 4.2 or 4.8 mg/mL enzyme stock was exchanged at least 4 times into pH 6.71 (25 mM MOPS); pH 7.51 (50 mM Tris); pH 8.00 (50 mM HEPPS), pH 8.51 (50 mM HEPPS); pH 9.27 (25 mM glycine) buffer in a 50 kDa filter. The volume of enzyme after the final exchange was 15 – 20 μL for a given pH ($\sim 1 - 3$ mM). The sample and reference (buffer) were then loaded into a split CaF_2 cell (described in the previous experimental section) with a 76 μm pathlength using a gas tight syringe.

Each sample was placed in the home-built external sample compartment of a Varian 660 FTIR spectrometer (described in the previous experimental section) and 4096 scans of the sample and reference were obtained at lab temperature ($\sim 20 \pm 1$ $^\circ\text{C}$) with 2 cm^{-1} resolution.

Infrared spectra were collected for the pH = 8.5 sample between 8 – 70 $^\circ\text{C}$ in the same sample compartment. The temperature was controlled by a circulating water bath and recorded by a homebuilt LabView program using a thermocouple attached to one face of the copper cell. 4096 scans of the sample and reference were collected for each temperature. The translation stage was rastered to the same sample/reference spot for each measurement by the LabView program.

To monitor the oxidation of R355K SH1, the pH = 9.27 sample was stored in a 4 $^\circ\text{C}$ refrigerator or kept at room temperature (~ 20 $^\circ\text{C}$) for thirty-two days, and the FTIR spectrum was measured periodically.

The native SH1 pH = 7.23 for comparison with R355K at pH = 7.23 (Figure 2, main text) were prepared similarly. The buffer used for native enzyme was 50 mM potassium phosphate / 50 mM MPA. The pathlength was 50 μm .

9. CO Incubated FTIR Samples

To prepare CO incubated R355K samples, 1 mL of 4.2 mg/mL of enzyme stock was exchanged into 50 mM, pH = 8.0 HEPPS buffer. To prepare WT and E17Q controls, $\sim 450 - 470$ μL of 6.4 mg /mL WT enzyme stock and 5.12 mg / mL of E17Q enzyme stock were exchanged into freshly prepared 50 mM, pH = 8.0 anaerobic HEPES buffer. Each sample as brought to a final volume of 20 – 25 μL and transferred to a gas tight, low volume vial (Verex™) and incubated under a CO atmosphere for 10 – 15 minutes outside of the anaerobic chamber (the volume was kept higher than usual to account for evaporation, which was typically ~ 5 μL). The enzyme was quickly transferred to the anaerobic chamber (~ 5 minutes) and loaded into a split CaF_2 cell containing a 76 μm spacer using a gas tight syringe. Enzyme concentrations were 1 – 2 mM.

10. Methyl Viologen Oxidation Reduction of Native and R355K Pf SH1 under 5% H₂ monitored via UV-Vis Spectroscopy

An aliquot of 2.8 mg/mL of native SH1 or 4.2 mg/mL of R355K SH1 was exchanged into pH = 7.2, 50 mM potassium phosphate buffer x 6. The given hydrogenase sample and a stock of methyl viologen were then diluted in a 1 x 1 cm quartz cuvette to working concentrations of 50 nM hydrogenase and 330 μM methyl viologen. In both cases the immediate appearance of blue from methyl viologen reduction was noted because of the $\sim 4\%$ H₂ gas composition of the buffer. The cuvette was then sealed with a rubber septum and removed from the anaerobic chamber and purged with a 5% H₂ / 95% N₂ gas mix for at least 50 minutes to ensure both samples had identical gas compositions. The septum was sealed with Teflon tape. Temperature dependent UV-Vis data were collected using the absorbance mode of a Horiba Scientific Dual Fluorimeter that was equipped with a Peltier temperature controller and magnetic stirrer. A 7 minute equilibration time was set for each point during the temperature ramp for a total collection time of ~ 1.5 hours. When the temperature was returned from 75 $^\circ\text{C}$ to 15 $^\circ\text{C}$, spectra were measured until no change was observed. The reference was a buffer spectrum.

Data Analysis

FTIR absorbance spectra, difference spectra, and corresponding baseline corrections were carried out with the Resolutions Pro software. Unless noted otherwise, the remaining data analysis utilized Igor Pro (Wavemetrics, Inc.; Lake Oswego, Oregon).

1. H/D Exchange

To calibrate the H/D exchange measurements, standards were utilized to observe where H₂, HD, and D₂ appeared on the CCD camera with the instrumental parameters utilized. For each standard, cosmic ray spikes were manually removed by replacing each spike with the average of two adjacent background points. An empty cuvette spectrum (blank) was analyzed identically and then subtracted from each standard. The baselines were then corrected with a spline function. The center pixel for each scatter spectrum was determined by a one component Voigt function and were assigned to the known Raman detectable stretching frequencies of H₂ (4160 cm⁻¹), HD (3632 cm⁻¹) and D₂ (2989 cm⁻¹).⁹ A linear correlation of wavenumber vs. pixel was then determined (**Figure S1**). The center pixel of H₂ (determined to be pixel 219) was manually set to 4160 cm⁻¹, and the remaining pixels were assigned a wavenumber relative to this value using the slope of the calibration curve (**Figure S1, inset**).

Each time point for a kinetics measurement was analyzed identically with cosmic ray spike removal, cuvette subtraction, and a spline baseline correction; an example is provided in **Figure S2**. Representative spectra for both native and R355K SH1 between 4 – 800 minutes of data collection are provided in **Figure S3**. The relative amount of H₂, HD, and D₂ in the headspace for a given time point was determined by integrating the peak area for each gas in the full width half maximum region as determined by the standards. Plots of the integrated areas versus time are shown for native and R355K SH1 in **Figures S4 and S5**, respectively. The summed total areas under the curve (D₂ + HD + H₂) for each time point averaged to 40000 +/- 1700 for native and 40000 +/- 1600 for R355K SH1, and thus there was no obvious gas loss during the measurements.

For a conservative analysis of the data, we applied the method of initial rates to the first 60 minutes of the measurements of D₂ consumption and HD production for native enzyme. This was also applied to D₂ consumption for R355K SH1. Because of weak signals from HD production at early time with R355K SH1 and the inherent noise of the measurements, the method of initial rates was applied to the first 180 minutes. Otherwise, rates that varied by up to a factor of two could be obtained at earlier times depending on the exact time point range. Furthermore, exponential fits were applied to the first 668 minutes of native SH1 HD production and to the entire data set of R355K, which did not display a notable HD decay (the observed HD decay from native enzyme is from HD in the gas phase eventually reacting the enzyme to form H₂ within the time course of the experiment at a detectable level). The fits are shown in **Figures S4 and S5** and the parameters are tabulated in **Table S1**. The maximum amount of HD produced by native enzyme was determined by the average of the data points between 500 and 600 minutes (**Table S2**). The maximum amount of HD produced by R355K enzyme was determined by the average of the final two data points (**Table S2**). We also provide the value of HD produced by the R355K enzyme at 800 minutes by averaging the data points at 796, 800, and 804 minutes.

We also estimated the amount of D₂ consumed. It was assumed the total scatter area of starting D₂ was 40,000. The final area (proxy for amount) of D₂ for the native enzyme was estimated as the average of the final five data points, and were divided by 40,000 (and multiplied by 100 and subtracted from 1) to get the percentage of D₂ consumed. The amount of D₂ consumed by R355K SH1 was estimated similarly. We also provide the percentage of D₂ consumed by R355K SH1 at 800 minutes by averaging the data points at 796, 800, and 804 minutes for the calculation.

The data for R355K was also scaled to account for concentration differences (a factor of 0.54) in **Figure 2** and in **Table S2**, which assumes a concentration linearity regarding the rates D₂ cleavage and HD and H₂ formation.

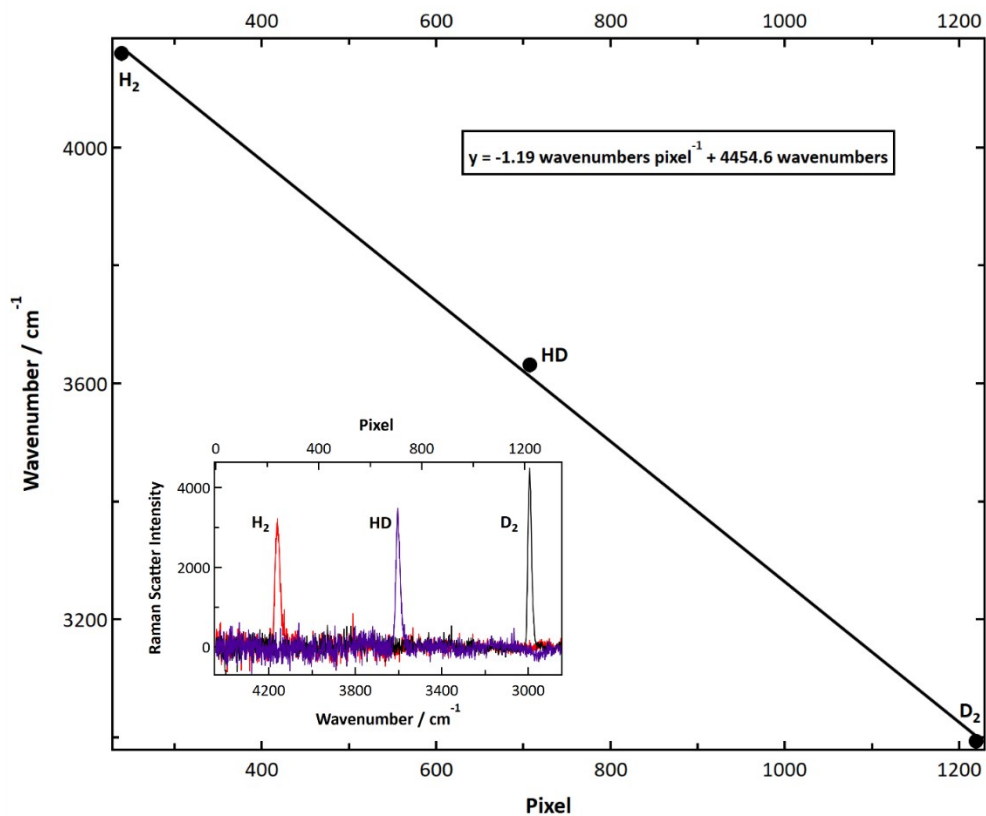


Figure S1: Linear relationship obtained for pixel number and Raman scatter position based on the peak position of D₂, HD, and H₂ gas standards. The wavenumber axis of the inset and in subsequent figures was generated by fixing the center pixel of H₂ as 4160 cm⁻¹ and using the slope of calibration curve to assign wavenumber values to the other pixels.

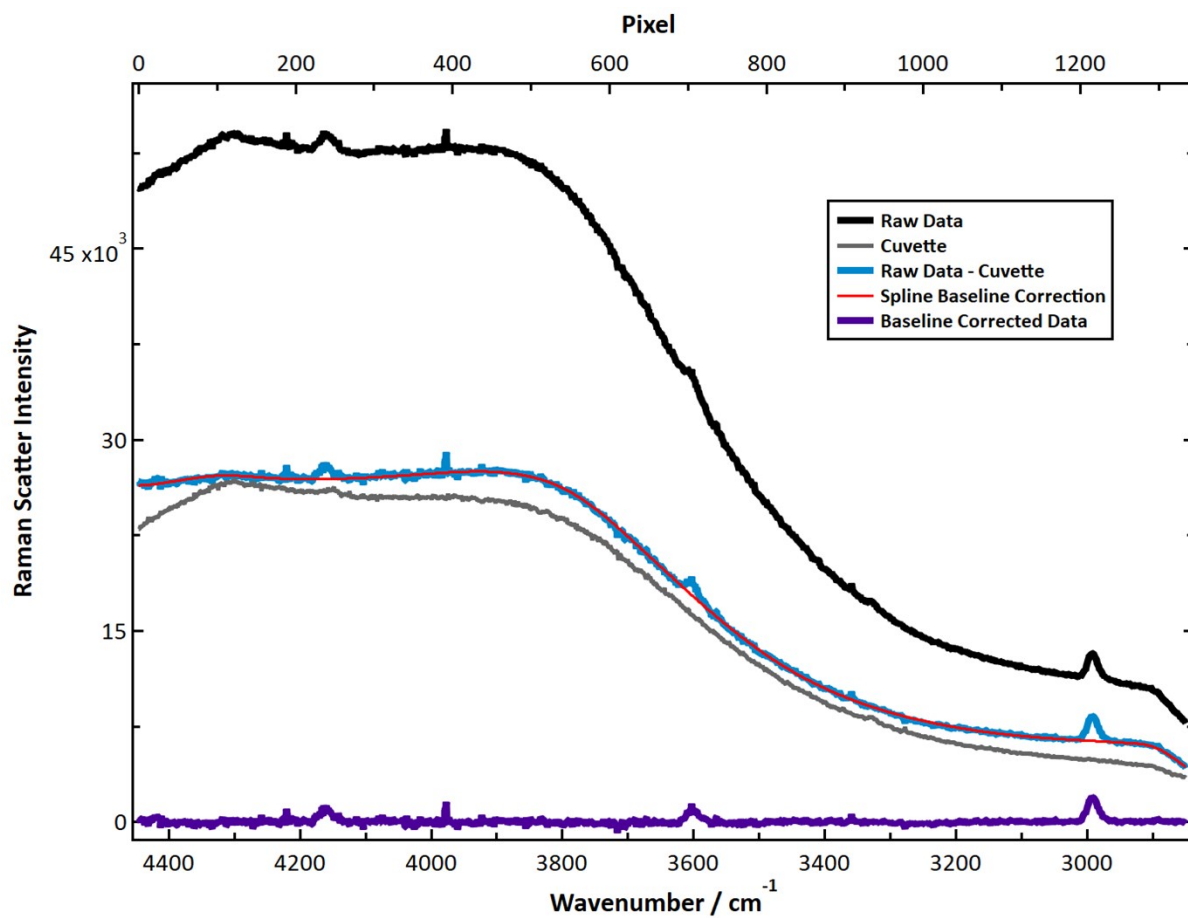


Figure S2: Example analysis of a Raman spectrum from an H/D exchange experiment for native SH1 using the data corresponding to 260 minutes.

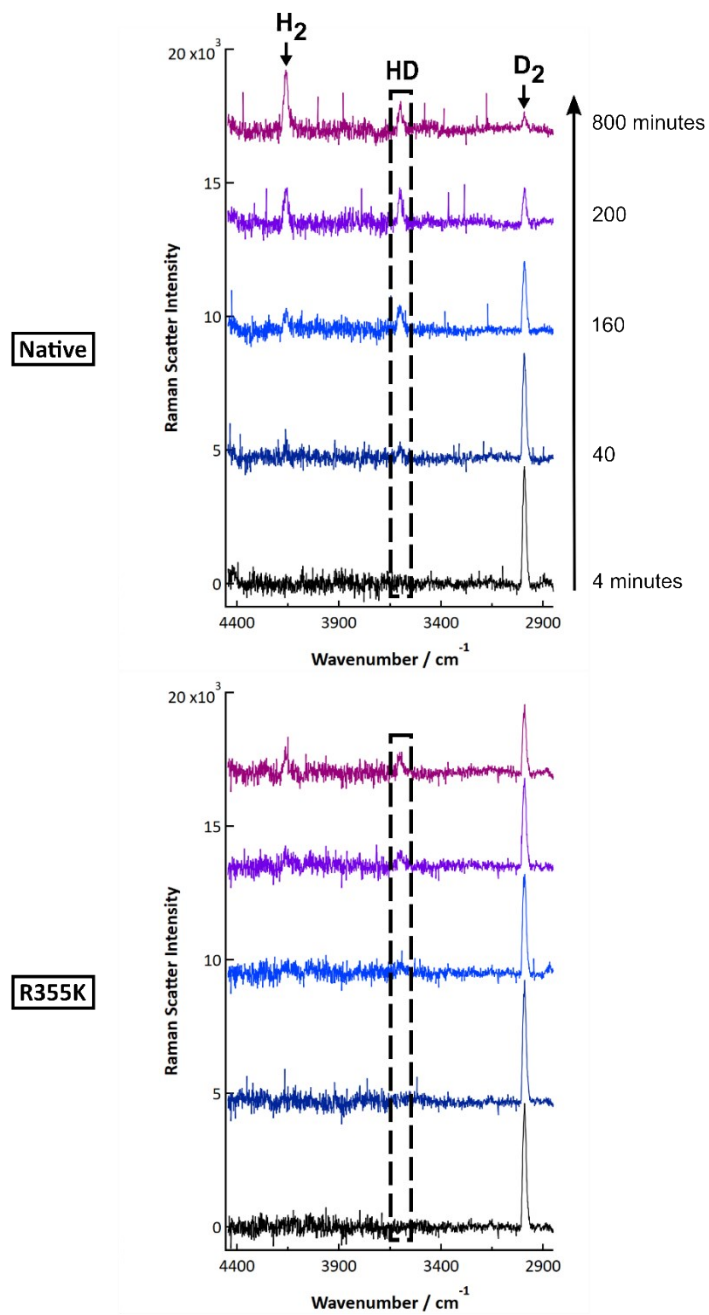


Figure S3: Time dependent Raman spectra of 222 nM native SH1 and 412 nM R355K SH1 during H/D exchange measurements from 4 – 800 minutes in 50 mM KP_i buffer, pH = 6.3, and 1.5 mM dithionite.

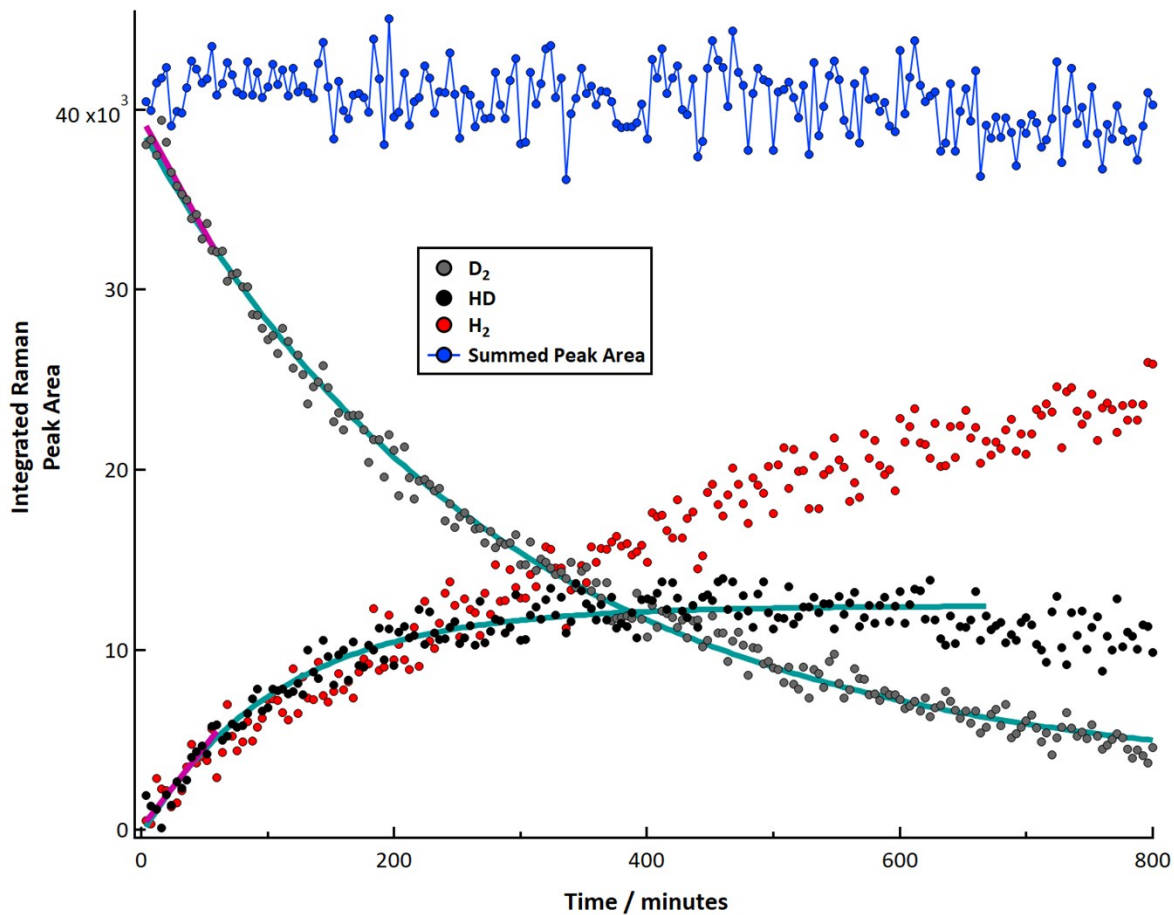


Figure S4: Time course of D_2 consumption and HD and H_2 production by 222 nM WT enzyme from plotting the integrated Raman scatter of the respective peaks at the full-width half maximum values obtained from the standards. The linear fits correspond to the first 60 minutes, and the exponential fit to the first 668 minutes of the assay for HD formation and 800 minutes for D_2 consumption. Results of the individual fits are provided in **Table S1**.

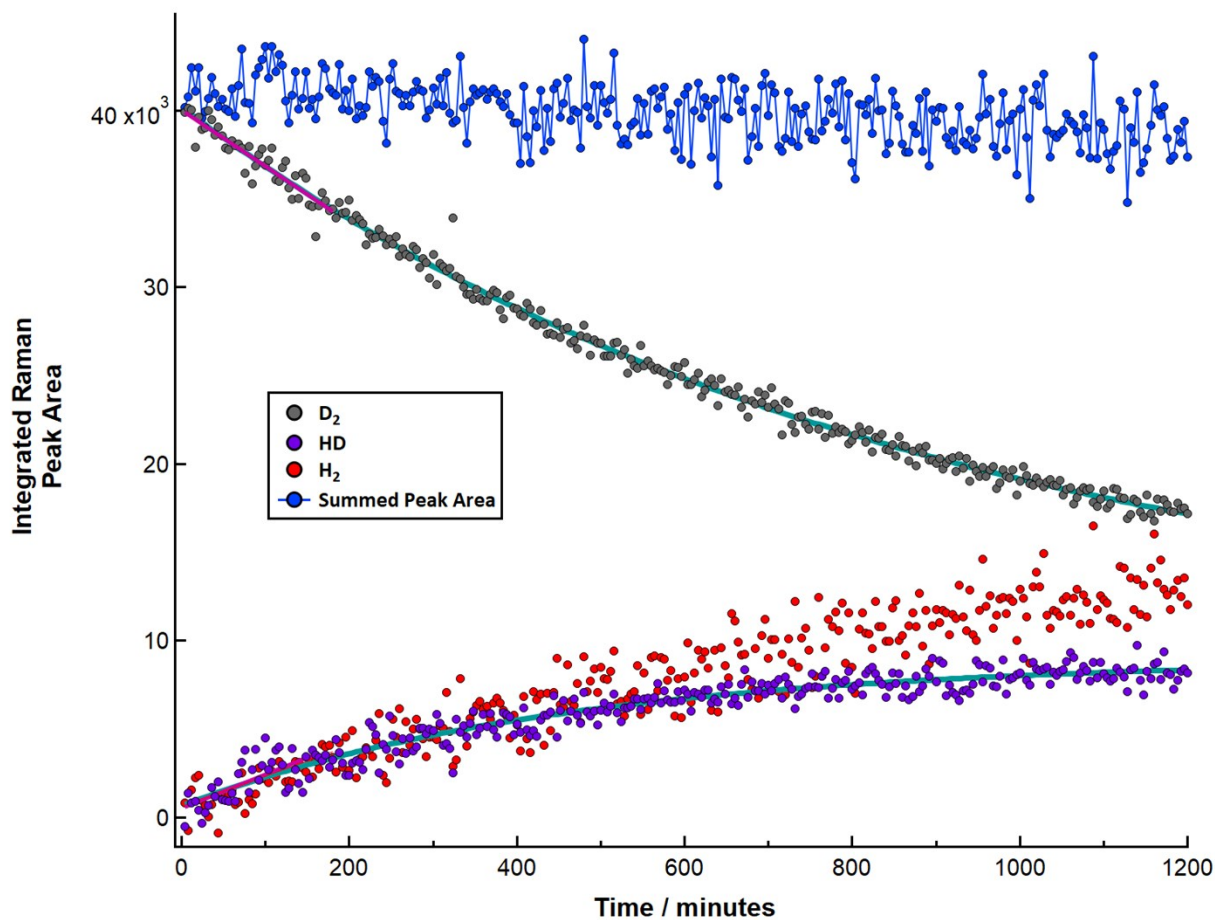


Figure S5: Time course of D_2 consumption and HD and H_2 production by 412 nM R355K enzyme from monitoring the integrated Raman scatter of the respective peaks at the full-width half maximum values obtained from the standards. The linear fits corresponds to the first 180 minutes, and the exponential fit to 1200 minutes. Results of the individual fits are provided in **Table S1**. Note: because of the small amount of H_2 produced (see **Figure S3**, for example), we anticipate much of the integrated peak area for H_2 at early time is just inherent noise from the measurements, which is why we precluded from quantitatively analyzing the H_2 production. However, as seen in **Figure S3**, H_2 is clearly detected at later time.

Table S1: Linear (method of initial rates for the first 60 minutes of data collection for native SH1 and 180 minutes of data collection for R355K SH1) and exponential fits to the integrated Raman scatter areas of D₂ and HD in **Figures S4 and S5** for native (222 nM) and R355K SH1 (412 nM). Errors are provided in parenthesis.

Enzyme	Linear (Slope) / Peak Area min ⁻¹	Linear Intercept / Peak Area	Exponential rate / min ⁻¹	Exponential Amplitude / Peak Area	Exponential Offset / Peak Area
Native, HD	89 (11)	90 (400)	9.2 (0.5) x 10 ⁻³	-13,000 (300)	12,000 (100)
R355K, HD	17.1 (3)	600 (300)	2.2 (0.13) x 10 ⁻³	-8,000 (200)	9,000 (200)
Native, D ₂	-127 (11)	40,000 (400)	3.5 (0.06) x 10 ⁻³	36,000 (200)	3,000 (200)
R355K, D ₂	-30 (2)	40,000 (200)	1.1 (0.03) x 10 ⁻³	30,000 (400)	10,000 (400)

Enzyme	Maximum HD Peak Area	Scaled HD Peak Area	Percentage of Starting D ₂ Consumed	Scaled Percentage of D ₂ Consumed
Native	12,200	-	90%	-
R355K	8,300 (1200 minutes) 7,700 (800 minutes)	4,500 (1200 minutes) 4,100 (800 minutes)	56% (1200 minutes) 47% (800 minutes)	30% (1200 minutes) 25% (800 minutes)

Table S2: Maximum amount of HD produced and the amount of D₂ consumed by native and R355K SH1.

2. Electron Paramagnetic Resonance Spectroscopy

A minimal baseline correction was applied to each spectrum. Using the MATLAB EasySpin toolbox (Pepper function),¹³ rhombic fits were applied to the paramagnetic nickel region ($g > \sim 2$); however, a given spectrum also consisted of a strong axial contribution(s) from additional cofactors such as the [2Fe2S] cluster in the γ -subunit, which has previously been observed in native SH1.¹⁴ The axial signal(s) overlap and effectively hide the typical Ni^{3+} and Ni^{1+} g_z features near $g = 2.01$ and 2.05 , respectively.^{15, 16} Thus, the value of g_z was fixed as 2.01 for all native SH1 spectral features and 2.045 for all R355K spectral features. Along with carefully selected g -strain (peak widths), these allowed for a proper baseline prior to the g_y region (in the work with *Pf* SH1 by Silva and co-workers regarding paramagnetic nickel species, g_z had been fixed to 2.0 for all spectral fits (tentative oxidized features and Ni_a^{3+-C}).¹⁴ The fits were conducted between 2500 - \sim 3400 Gauss. Line broadening was accounted for by g -strain. The resultant spectra for native and R355K are provided in **Figure S6 – Figure S9**. The g -values obtained from the fits are provided in **Tables S3 – S6**.

In **Figure 3**, the maximum value of g_y for the data as fit in EasySpin were scaled/normalized to 1, and the corresponding fits scaled by the same value. For native SH1, the scaling values were 7 (pH = 6.7) and 24 (pH = 9.3). For R355K SH1, the scaling values were 205 (pH = 6.7) and 352 (pH = 9.3).

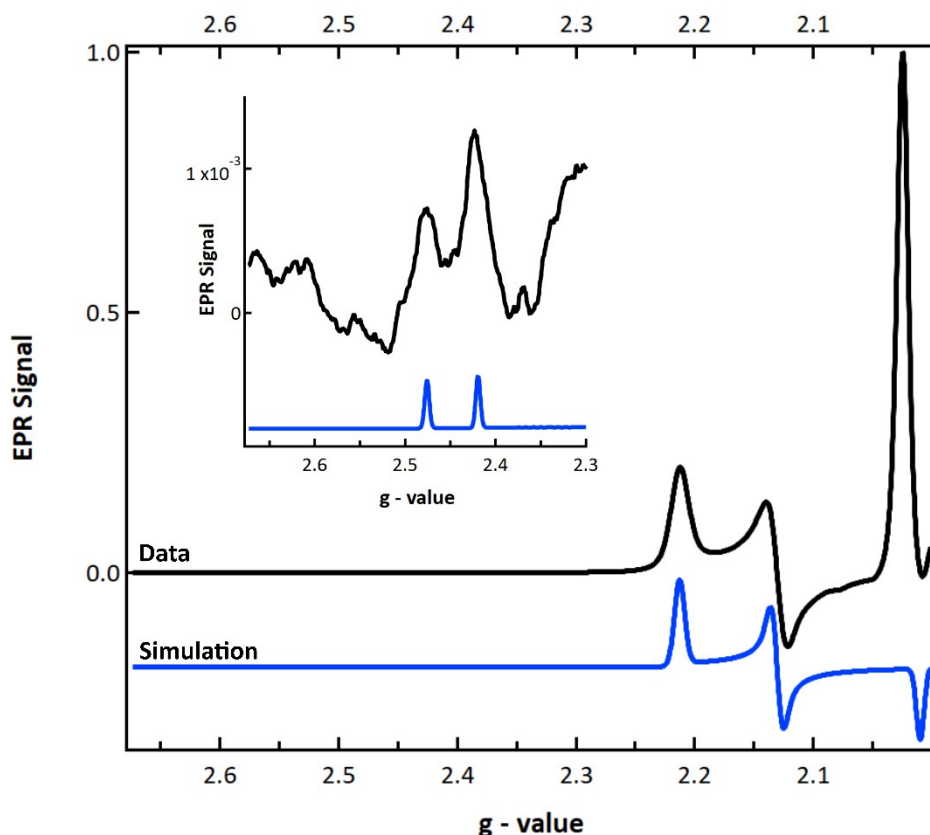


Figure S6: EPR spectrum of ~ 0.13 mM native SH1 at pH = 6.7. The temperature was 70 K. The modulation frequency was 100 kHz, the modulation amplitude was 0.4 mT, and the microwave power was 10 mW. The data represent an average of 100 scans. The inset displays two weak species observed with $g_x \sim 2.4 - 2.5$. Silva and coworkers previously observed a ready but inactive state with $g_x \sim 2.48$ in *Pf* SH1 termed “Ready”,¹⁴ and the two very minor states observed here may be similar to these “Ready” states. The simulated data has been offset for clarity.

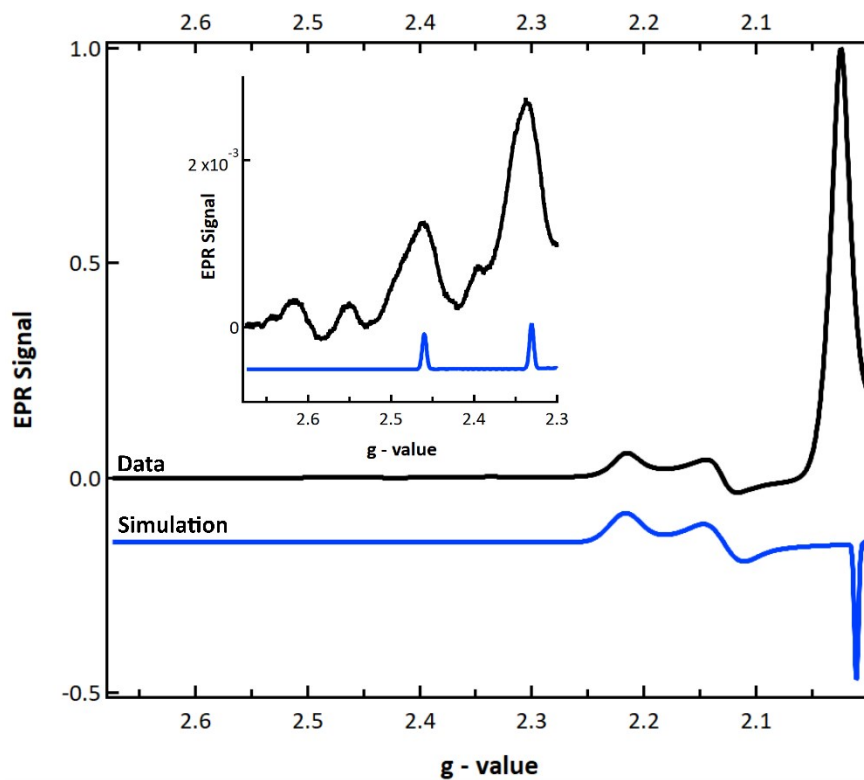


Figure S7: EPR spectrum of ~ 0.13 mM native SH1 at pH = 9.3. The temperature was 70 K. The modulation frequency was 100 kHz, the modulation amplitude was 0.4 mT, and the microwave power was 10 mW. The data represent an average of 500 scans. The inset displays two weak species observed with $g_x \sim 2.3 - 2.5$. The two minor states show in the inset may be similar to the “Ready” and “Unready” state observed by Hagen and co-workers (see also **Table S7**).¹⁴ The simulated data has been offset for clarity.

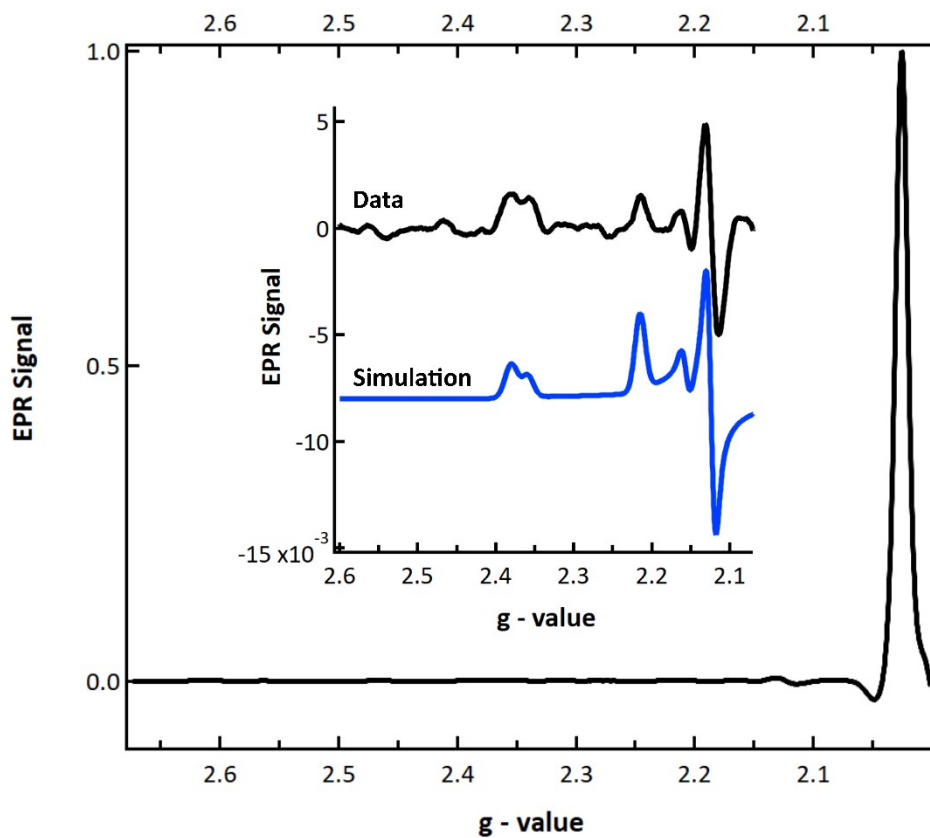


Figure S8: EPR spectrum of ~ 0.8 mM R355K SH1 at pH = 6.7. The temperature was 50 K. The modulation frequency was 100 kHz, the modulation amplitude was 0.4 mT, and the microwave power was 10 mW. The data represent an average of 225 scans. The inset displays the relevant g_y and g_x region and the corresponding three component axial spectral fit. The simulated data has been offset for clarity.

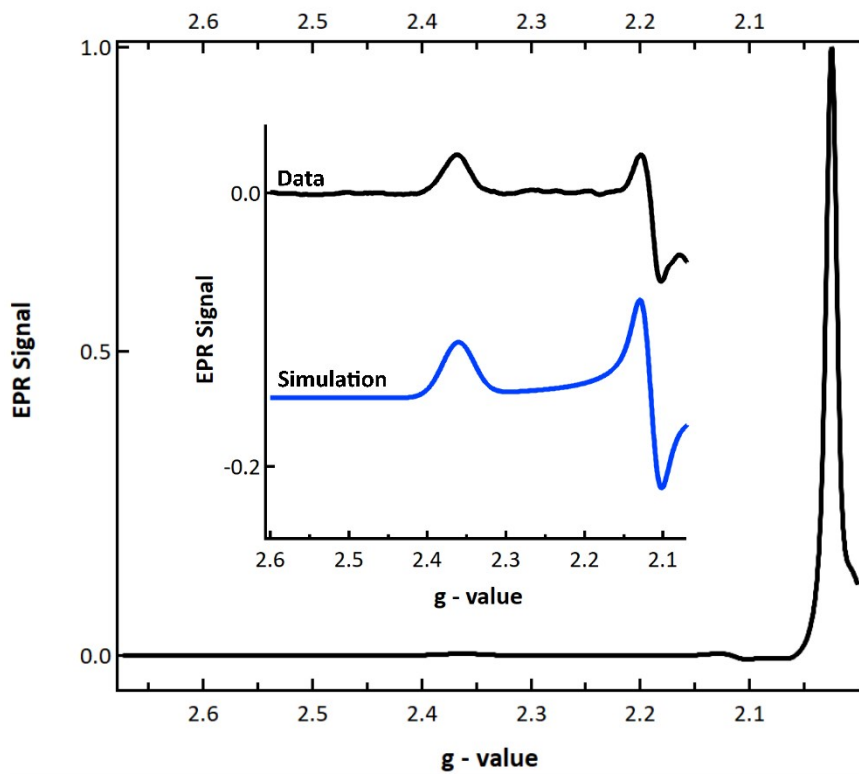


Figure S9: EPR spectrum of ~ 0.8 mM R355K SH1 at pH = 9.3. The temperature was 50 K. The modulation frequency was 100 kHz, the modulation amplitude was 0.4 mT, and the microwave power was 10 mW. The data represent an average of 100 scans. The inset displays the relevant g_y and g_x region and the corresponding minimal one component axial spectral fit. The simulated data has been offset for clarity.

Table S3. Native *Pf* SH1 at pH = 6.7; g – values determined from a three component rhombic EPR fit. The corresponding g -strains (peak widths) are provided in parenthesis.

State, pH = 6.7	g_z	g_y	g_x
Ni_a^{3+} -C	2.010 (0.0075)	2.131 (0.01)	2.218 (0.01)
Ni_r^{3+} -B like ¹	2.010 (0.0075)	2.131 (0.0095)	2.420 (0.0055)

pH / state	Ni_a^{3+} -C	Ni_r^{3+} -B like	Ni_u^{3+} -X	Ref.
6.7	2.01, 2.131, 2.218	2.01, 2.131, 2.420 2.01, 2.130, 2.476	-	This work
8.0	2.0, 2.137, 2.2185	2.0, 2.127 (0.035), 2.389 (0.120)	2.0, 2.147 (0.004), 2.304 (0.006)	¹⁴
9.3	2.04, 2.128, 2.217	2.04, 2.128, 2.456	2.01, 2.128, 2.330	This work
Ni_r^{3+} -B like	2.010 (0.0075)	2.130 (0.0095)	2.476 (0.0055)	

Table S4. Native *Pf* SH1 at pH = 9.3; g – values determined from a three component rhombic EPR fit. The corresponding g -strains (peak widths) are provided in parenthesis.

State, pH = 9.3	g_z	g_y	g_x
Ni_a^{3+} -C	2.010 (0.0035)	2.128 (0.033)	2.217 (0.032)
Ni_u^{3+} - X	2.010 (0.0035)	2.128 (0.032)	2.330 (0.0055)
Ni_r^{3+} -B like	2.010 (0.0035)	2.128 (0.032)	2.456 (0.0055)

Table S5. R355K *Pf* SH1 at pH = 6.7 g – values determined from a three component rhombic EPR fit. The corresponding g -strains (peak widths) are provided in parenthesis.

State, pH = 6.7	g_z	g_y	g_x
Ni_a^{+} -L1	2.045 (0.008)	2.124 (0.0115)	2.380 (0.0189)
Ni^{3+} -X	2.045 (0.008)	2.156 (0.0115)	2.359 (0.0170)
Ni_a^{3+} -C	2.045 (0.008)	2.124 (0.0115)	2.215 (0.0155)

Table S6. R355K *Pf* SH1 at pH = 9.3 g – values determined from a rhombic EPR fit using a minimal one component system. The corresponding g -strains (peak widths) are provided in parenthesis.

State, pH = 9.3	g_z	g_y	g_x
Ni_a^{+} -L	2.045 (0.0025)	2.116 (0.025)	2.362 (0.047)

¹Tentative oxidized states observed by our laboratory in native SH1 displayed very weak signals that were only clear in the g_x region (see **Figures S6 – S7**).

Table S7. Summary of native *Pf* SH1 active site EPR studies. Values and errors (standard deviation) for pH = 8.0 represent errors from various enzyme treatments explored by Silva co-workers, except for the $\text{Ni}_a^{3+}\text{-C}$ which was only observed at $T = 80^\circ\text{C}$. Our current preparation, storage, and activation methods have allowed for ample $\text{Ni}_a^{3+}\text{-C}$ to be observed by FTIR under mild conditions (and EPR studies in this work). The source of discrepancy between the different results of the two laboratories is not clear. The redox states are presumed to be 3+ for all features because, to the best of our knowledge, paramagnetic oxidized/inactive features are formally 3+ for all [NiFe]-hydrogenases.^{15, 16} The g-values are listed in the order of g_z, g_y, g_x .

Table S8: Tabulation of g – values of $\text{Ni}_a^{3+}\text{-C}$ and $\text{Ni}_a^{+}\text{-L}$ from various [NiFe]-hydrogenases and the corresponding $g_y(\text{Ni}_a^{3+}\text{-C}) - g_y(\text{Ni}_a^{+}\text{-L})$ value and $g_x(\text{Ni}_a^{3+}\text{-C}) - g_x(\text{Ni}_a^{+}\text{-L})$ values, which were used to ultimately identify the paramagnetic state(s) in R355K SH1. The g – values are listed in the order of: g_z, g_y, g_x . Each enzyme group and subgroup is also provided.^{17, 18}

Enzyme source	Group	$\text{Ni}_a^{3+}\text{-C}$	$\text{Ni}_a^{+}\text{-L}$	$g_y(\text{Ni}_a^{+}\text{-C}) - g_y(\text{Ni}_a^{3+}\text{-L})$	$g_x(\text{Ni}_a^{3+}\text{-C}) - g_x(\text{Ni}_a^{+}\text{-L})$	Ref.
---------------	-------	-----------------------------	----------------------------	--	--	------

<i>Allochrochromatium vinosum</i> ¹	1e	2.01, 2.15, 2.21	2.05, 2.12, 2.26 2.05, 2.12, 2.28	0.03	-(0.05 - 0.07)	15, 19
<i>Wolinella succinogenes</i>	1b	2.01, 2.15, 2.195	2.045, 2.125, 2.295 nd, 2.15, 2.265	(0 - 0.025)	-(0.07 - 0.1)	20
<i>Thiocapsa roseopersicina</i>	1e	2.02, 2.15, 2.19	2.05, 2.13, 2.29	0.02	- 0.10	21
<i>Desulfovibrio vulgaris</i> Miyazaki F	1a	2.01, 2.142, 2.20	2.049, 2.116, 2.30 n.d., n.d., 2.321	0.026	-(0.10 - 0.121)	15, 22-24
<i>Desulfovibrio gigas</i>	1a	2.009, 2.146, 2.192	2.044, 2.113, 2.264 2.045, 2.124, 2.293 n.d., 2.16, 2.41	(-0.0140 - 0.033)	-(0.072 - 0.218)	25-27
<i>Desulfovibrio fructosovorans</i>	1b	2.009, 2.146, 2.192	2.044, 2.113, 2.264 2.045, 2.124, 2.293	(0.022 - 0.033)	-(0.072 - 0.101)	26
<i>Aquifex aeolicus</i> hydrogenase-1	1d	2.01, 2.15, 2.21	2.05, 2.15, 2.33 2.05, 2.12, 2.28	(0.00 - 0.03)	-(0.07 - 0.12)	28
<i>Escherichia coli</i> hydrogenase-1	1d	2.01, 2.14, 2.21	2.05, 2.14, 2.33	0.00	- 0.12	29, 30
<i>Ralstonia eutropha</i> H16 trimer ³ (membrane bound hydrogenase)	1d	2.01, 2.14, 2.20	2.05, 2.11, 2.30 2.05, 2.11, 2.27 2.05, 2.11, 2.24	0.03	-(0.04 - 0.10)	31
<i>Ralstonia eutropha</i> H16 (cytoplasmic H ₂ sensor)	2b	2.015, 2.139, 2.197	2.046, 2.094, 2.251 2.054, 2.077, 2.305	(0.045 - 0.062)	-(0.054 - 0.108)	32, 33
<i>Ralstonia eutropha</i> H16 (cytoplasmic NAD ⁺ - linked)	3d	2.016, 2.139, 2.208	2.051, 2.105, 2.281	0.034	-0.073	34
<i>Acidithiobacillus ferrooxidans</i> ⁴	2a	2.008, 2.150, 2.215	2.038, 2.116, 2.276	0.034	-0.061	15, 35
<i>Pyrococcus furiosus</i> soluble hydrogenase -1, <i>prior work</i>	3b	n.d., 2.137, 2.2185	n.o.	n.d.	n.d.	14

<i>Average</i>	0.025	-0.09
<i>Standard Deviation</i>	0.016	0.04

<i>Pyrococcus furiosus</i> soluble hydrogenase -1 ⁶	3b	n.d., 2.13, 2.22	n.d., 2.12, 2.36/8	0.01	-(0.14 - 0.16)	This work
---	----	------------------	--------------------	------	----------------	-----------

n.d. : not determined; n.o: not observed

¹ Previously referred to as *Chromatium vinosum*.

³ The trimeric is membrane bound and remains associated with the natural redox partner cytochrome b; when isolated from the membrane, the enzyme is a soluble dimer. For the dimer, the g values are (2.01, 2.14, 2.20) for Ni_a³⁺ - C and (2.05, 2.10, 2.25) for Ni_a⁺ - L.³¹

⁴ For the isolated enzyme. Whole cell values are: (2.10, 2.149 and 2.212) for Ni_a³⁺ - C and (2.039, 2.116, 2.275) for Ni_a⁺ - L.³⁵

⁵ Ni_a⁺ - L signals are from the R355K variant.

3. Fourier Transform Infrared Spectroscopy, Equilibrium Photochemical Reduction of R355K SH1

FTIR difference spectra from the equilibrium photochemical reduction were obtained by subtracting the dark sample spectrum from each illuminated sample spectrum ($\Delta A = -\log(I_{\text{light}}/I_{\text{dark}})$). A minimal baseline spline correction was applied between

1860–1907.5, 1980–2030, and 2110–2200 cm^{-1} (6 points total) because we observed a small baseline drift relative to the dark spectrum. The baseline corrected spectra were then vertically offset to 0 O.D. at 1880 cm^{-1} .

FTIR absorbance spectra from the photoreduction were obtained by subtracting the reference solution from each illuminated spectrum ($A = -\log(I_{\text{sample}}/I_{\text{reference}})$). Because of significant water content differences between the sample and reference, a minimal spline correction was applied between $\sim 1860–1907.5$; $1970–2030$; and $2100–2200 \text{ cm}^{-1}$, which are removed from the ν_{CO} and ν_{CN} region as evidenced in the second derivative spectra. The baseline corrected spectra were vertically offset to 0 O.D. at 1880 cm^{-1} . The second derivatives of the spectra are plotted in **Figure S10** between 1800–2200 cm^{-1} , and the absorbance spectra of the ν_{CO} region is plotted in **Figure S11**.

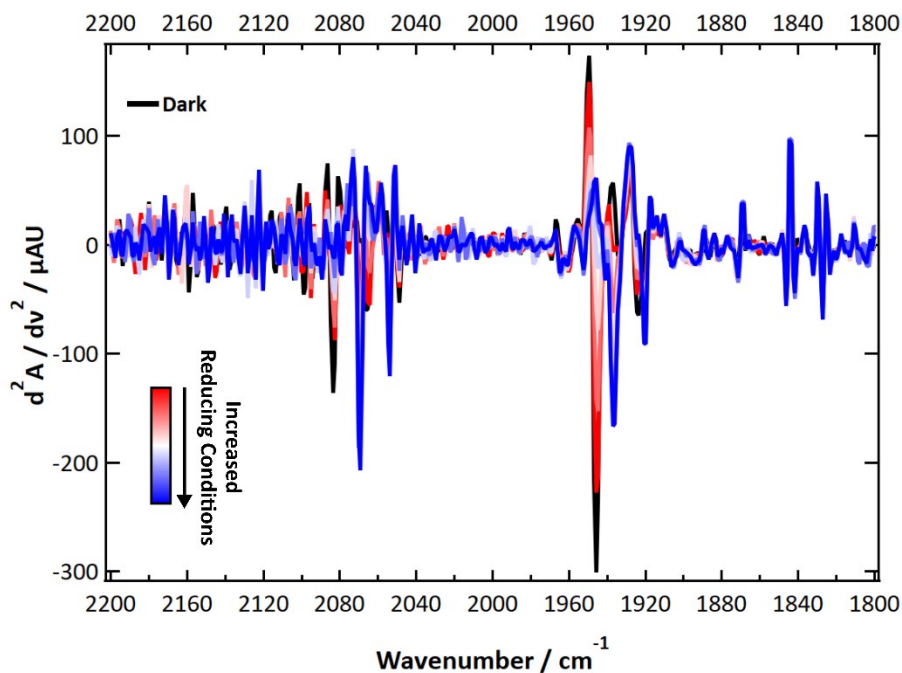


Figure S10: Second derivatives of the FTIR absorbance spectra collected during the steady state photochemical potential jump of R355K SH1 *prior* to performing a baseline correction. The initial conditions (dark, black spectrum) were 4 +/- 1 % hydrogen and $\sim 95\%$ nitrogen in 30 mM KPi / 50 mM MPA (sacrificial electron donor) pH = 7.2 buffer.

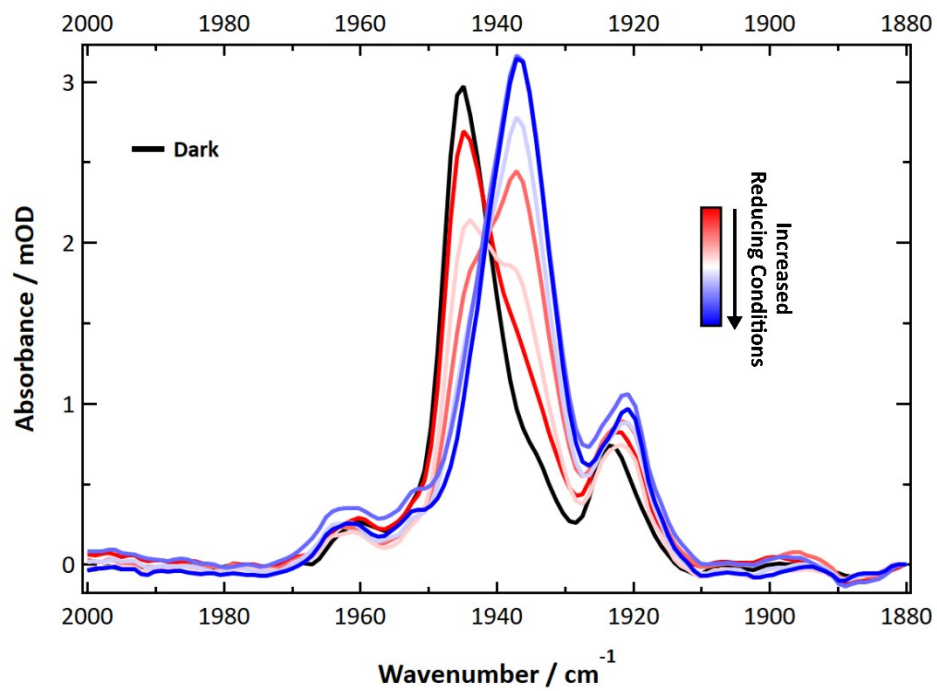


Figure S11: FTIR absorbance spectra collected during the steady state photochemical potential jump of R355K SH1. The initial conditions (dark, black spectrum) were 4 +/- 1 % hydrogen and ~ 95% nitrogen in 30 mM KP_i / 50 mM MPA (sacrificial electron donor) pH = 7.2 buffer.

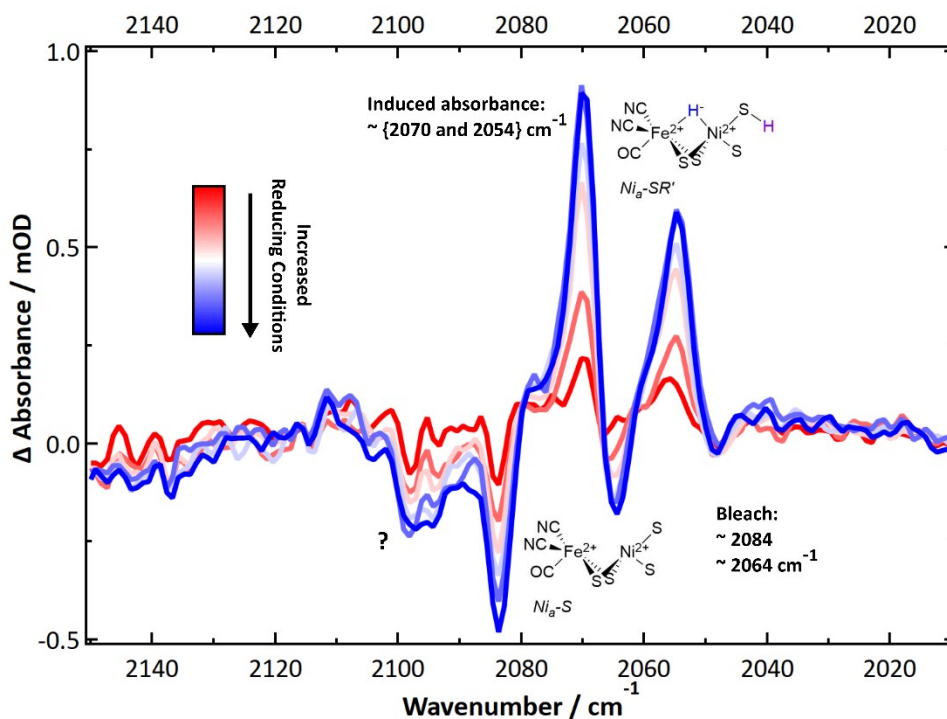


Figure S12: Difference spectra (light – dark) during the steady state photochemical potential jump from the ν_{CN} region. The spectra are from the data set used in **Figure 4b**. The data in **Figure 4b** show a clear bleach of $\text{Ni}_a^{2+}\text{-S}$ and a clear induced absorbance of $\text{Ni}_a^{2+}\text{-SR}'$. We accordingly assign the clear bleach at 2084 cm^{-1} to one of the CN stretches for $\text{Ni}_a^{2+}\text{-S}$, and the clear absorbances near 2070 and 2054 cm^{-1} to the symmetric and antisymmetric CN stretches for $\text{Ni}_a^{2+}\text{-SR}'$. The bleach near 2064 could correspond to $\text{Ni}_a^{2+}\text{-S}$ (as the antisymmetric CN stretch). The possible bleach(es) near $2090\text{--}2100 \text{ cm}^{-1}$ marked with a “?” could correspond to $\text{Ni}_a^{2+}\text{-S}$ or signals overlapped with $\text{Ni}_a^{2+}\text{-S}$ that are not resolved in the absorbance spectra and ν_{CN} region. An additional discussion of the CN bands is provided in an “Additional Analysis” section at the end of the Supplementary Information. Because of the extreme spectral overlap, the ν_{CN} values may be distorted/shifted and are only approximate.

4. Fourier Transform Infrared Spectroscopy of pH Dependent Samples

FTIR absorbance spectra for the pH dependent measurements were obtained by subtracting a given reference spectrum from the sample spectrum ($A = -\log(I_{\text{enzyme}}/I_{\text{reference}})$). The second derivative spectra are shown in **Figure S13**. A minimal baseline spline correction as applied between 1860 – 1907.5; 1972 – 2030; and 2100 – 2200 cm^{-1} (not overlapping with the ν_{CO} or ν_{CN} region as determined from second derivative spectra; 4 to 6 points were used in each region). The baseline corrected spectra were then offset to 0 OD at 1880 cm^{-1} . The resultant absorbance spectra are plotted in **Figure S14**.

The absorbance spectra were normalized to have the area under the curve (AOC) between 1880 – 2000 cm^{-1} equal to 1. The AOC (pre-normalized) for each pH value is presented in **Table S9**. The normalized spectra were fit to the ν_{CO} region using a multipeak Voigt function, **equation 1**:

$$f(\nu) = y_o + \sum_i A_i * g_i * e^{\left(\frac{\nu - \nu_i}{w_i}\right)^2} + A_i * (1 - g_i) * \frac{1}{1 + \left(\frac{\nu - \nu_i}{\frac{w_i}{2}}\right)^2} \quad (1)$$

where y_o is the linear offset, A_i is the amplitude, g_i is the Gaussian character (0 – 1), ν_i is the center frequency, and w_i the peak width at full width half maximum (FWHM) of the i^{th} peak. The peak widths were held constant for the peaks detected between 1900 – 1954 cm^{-1} as $w_i = 4 \text{ cm}^{-1}$. One (perhaps two) peaks was consistently detected at $\nu_{\text{CO}} > 1955 \text{ cm}^{-1}$ that was incredibly broad and difficult to define even in the second derivative spectra, and this width was constrained below 7 cm^{-1} . The individual fits and corresponding second derivative spectra are provided in **Figure S15 – S20**. The center frequencies for each peak are provided in **Table S10**.

In our prior work with native *Pf* SH1, analysis of FTIR data primarily focused on well-defined peak positions, specifically the $\text{Ni}_a^{3+}\text{-C}$ state that appears in a spectrally uncongested region between $\sim 1960 - 1970 \text{ cm}^{-1}$ (see also **Figure 4a**).^{2, 12} Unfortunately, the extreme spectral congestion in the R355K spectra precluded further analysis based primarily on peak positions. As previously noted for the peak position of $\text{Ni}_a^{2+}\text{-S}$ in native SH1 following sample preparation under the same conditions used here, exact peak positions are not well defined in spectrally congested regions,¹² especially for shoulder peaks. This is further complicated by the pH dependent peak position shifts that are the results of deprotonation of amino acid residues near the active site and increased population of reduced proximal iron-sulphur clusters as pH increases.^{2, 12, 36} Thus, there is some significant error/variability in peak positions depending on pH and if a given feature is a shoulder or more well defined feature (see **Table S10**). We thus further analysed the FTIR data based on a peak areas at full-width half maximum.

The population of each state at a given pH was estimated by integrating the intensity of each spectral feature using **equation 2**:

$$\text{Population}(\text{Ni}_{a/x}\text{-state}) = \int_{\nu_i - w_i}^{\nu_i + w_i} A_i * g_i * e^{\left(\frac{\nu - \nu_i}{w_i}\right)^2} + A_i * (1 - g_i) * \frac{1}{1 + \left(\frac{\nu - \nu_i}{\frac{w_i}{2}}\right)^2} \quad (2)$$

where all terms are determined from the fits to **equation 1**, and $\text{Ni}_o\text{-state}$ corresponds to an active state of the enzyme, while $\text{Ni}_x\text{-state}$ corresponds to what we believe to be an inactive state of the enzyme. These populations are presented in **Table S11**. The populations were then scaled relative to the $\text{Ni}_a^{+}\text{-L}$ states to account for the decreased ν_{CO} oscillator strength as frequency increases; the scaling factors were based on the work of Alben and co-workers.³⁷ The scaled populations are presented in **Table S12**.

The estimated H_2/H^+ redox couple for a given pH value is was calculated with **equation 3**³⁸ assuming a 4% hydrogen composition (the precise gas composition depends on how much time has passed between sample removal from the anaerobic chamber and how tight the ports of the infrared cell are sealed, both of which contribute to hydrogen escaping from the cell prior to a measurement):

$$E = 0 \text{ V} - \left(\frac{2.303 * R * T}{F} * pH \right) - \left(\frac{2.303 * R * T}{2F} * \log \left(\frac{\rho_{H_2}}{\rho_0} \right) \right) \quad (3)$$

where 0 V is the H₂/H⁺ couple at pH = 0, F is Faraday's constant (96,485 Coulombs/mol), T is the lab temperature (assumed to be the typical value of ~ 20 °C (293.15 K) in the specific location where the measurements are made as indicated by past measurements of the air temperature with a thermocouple), R is the gas constant 8.314 J/molK, and ρ_{H₂} is the partial pressure of hydrogen and ρ₀ is standard pressure.

To obtain absorbance spectra of the temperature dependent samples, the reference spectrum for a given temperature was subtracted from the sample spectrum of the same temperature ($A = -\log(I_{\text{sample, temperature } x} / I_{\text{reference, temperature } x})$). The absorbance spectra from 8 – 70 °C are provided in **Figure S22**. The spectra were fit using **equation 1** to non-normalized spectra with similar parameters as the pH dependent samples. The average peak position values of the Ni_a²⁺-S and Ni_a²⁺-SR' features are labeled in **Figure S21**.

The day dependent spectra for the pH = 9.27 sample were processed in the same manner as the pH dependent samples as described above, except more oxidized samples were normalized between 1880 – 2030 cm⁻¹ to account for the peak that appeared near 2012 cm⁻¹. Because of the appearance of additional peaks near 2012 and perhaps 2000 cm⁻¹, the spline region typically used between from 1972 – 2030 cm⁻¹ was broken into two components: 1978 – 1990 and 2020 – 2030 cm⁻¹. Broad peaks between 1950 – 1975 often required peak widths to be fixed at 5.5 cm⁻¹ in this region. The second derivative spectra are plotted in **Figure S22** and the normalized absorbance spectra are plotted in **Figure S23**. The normalization values are provided in **Table S13** and the peak positions in **Table S14**.

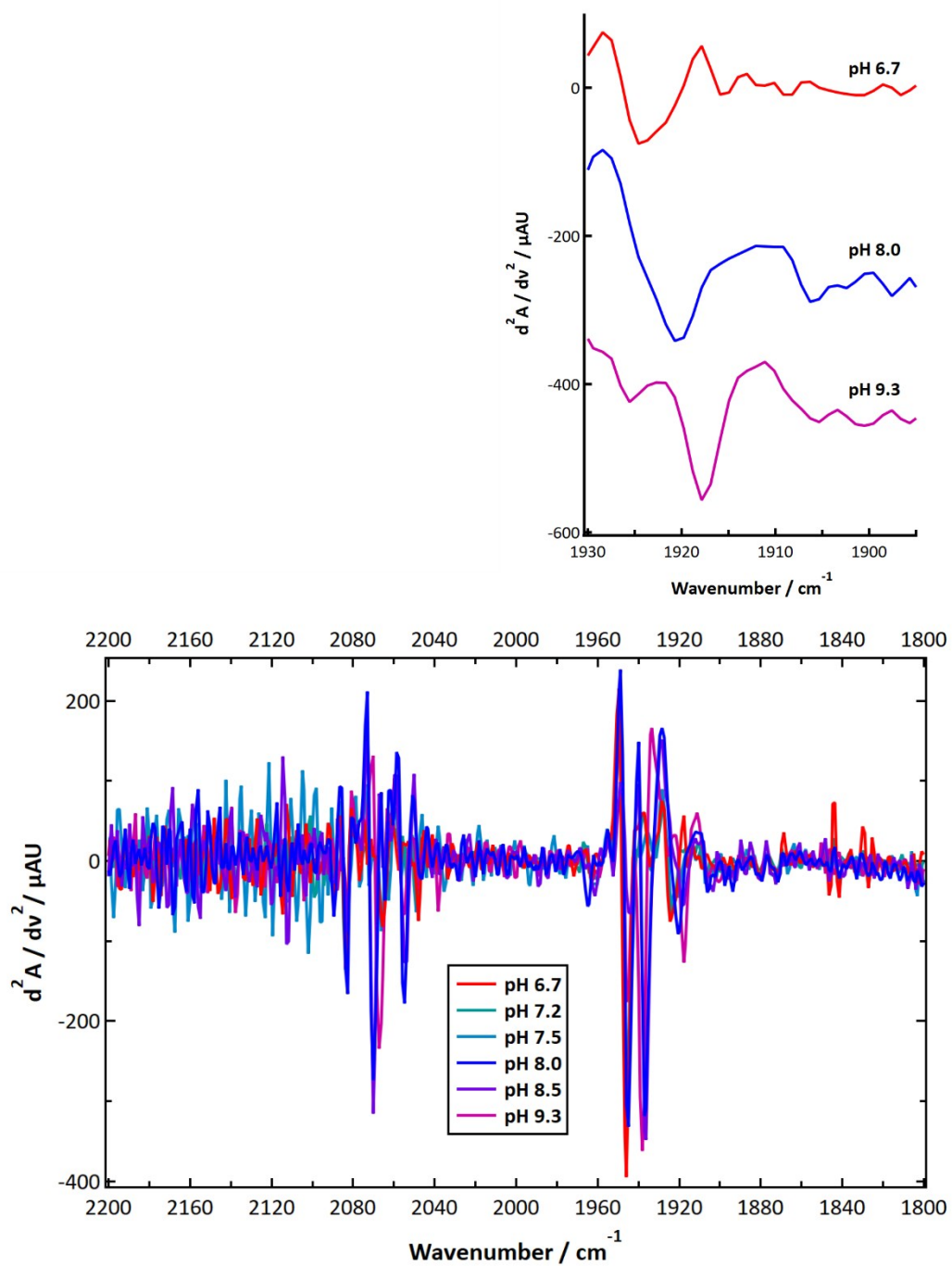


Figure S13: Second derivatives of the FTIR spectra prepared under $\sim 4 \pm 1\%$ hydrogen from between pH 6.7 and pH 9.3 from data *prior* to performing a baseline correction. Inset: zoomed in version of the $\text{Ni}_a^{+}\text{-L}$ region for pH = 6.7, 8.0, and 9.3; offsets were added for clarity.

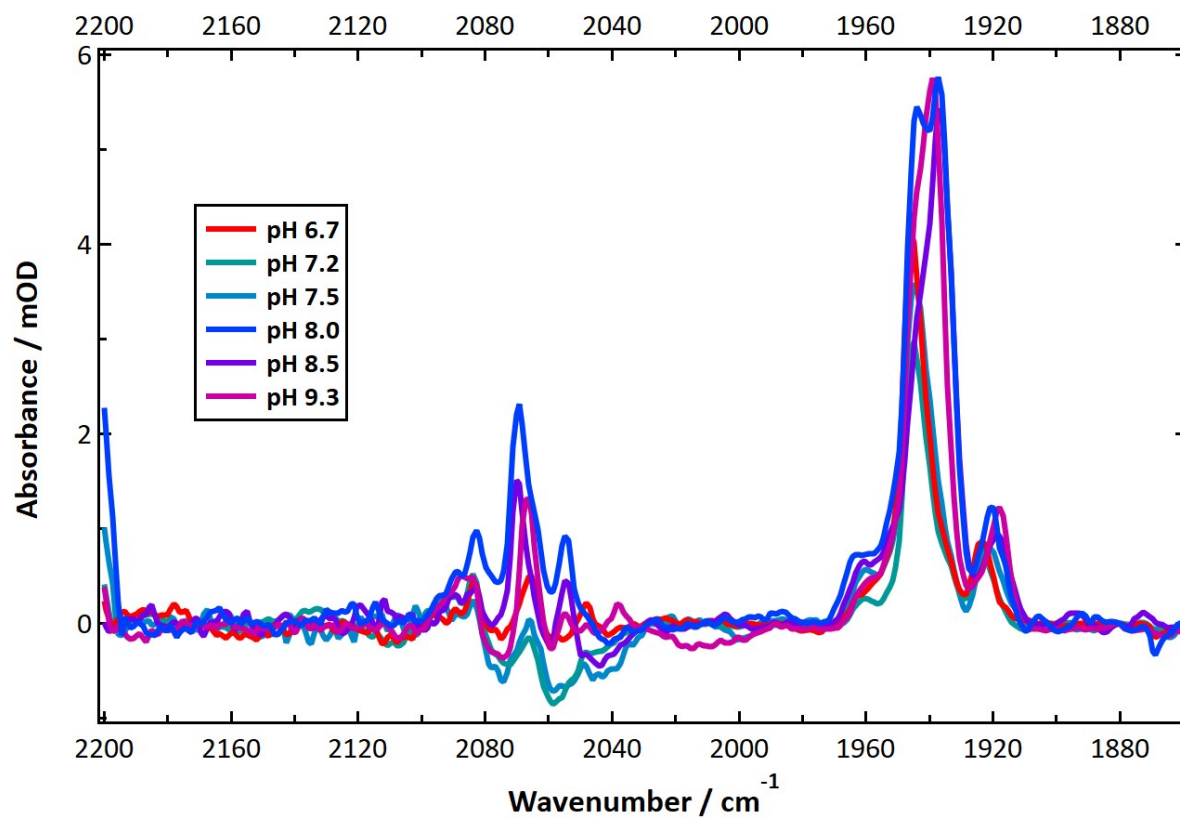


Figure S14: Baseline corrected FTIR spectra in the ν_{CO} ($\sim 1900 - 1980 \text{ cm}^{-1}$) and ν_{CN} region ($\sim 2040 - 2090 \text{ cm}^{-1}$) of R355K SHI enzyme as prepared under $\sim 4 \pm 1 \%$ hydrogen between pH 6.7 and pH 9.3. *Note:* to be consistent, we decided to apply the baseline spline correction to the same region for each sample. This unfortunately led to negative feature artifacts in the ν_{CN} region of some samples.

Table S9: Area under the curve (AOC) used for normalization for each IR spectrum between 1880 – 2000 cm^{-1} after baseline correction and offset of the absorbance to 0.0 O.D. at 1880 cm^{-1} .

pH	AOC, 1880 – 2000 cm^{-1}
6.7	0.0547
7.2	0.0394
7.5	0.0551
8.0	0.117
8.5	0.0921
9.3	0.0871

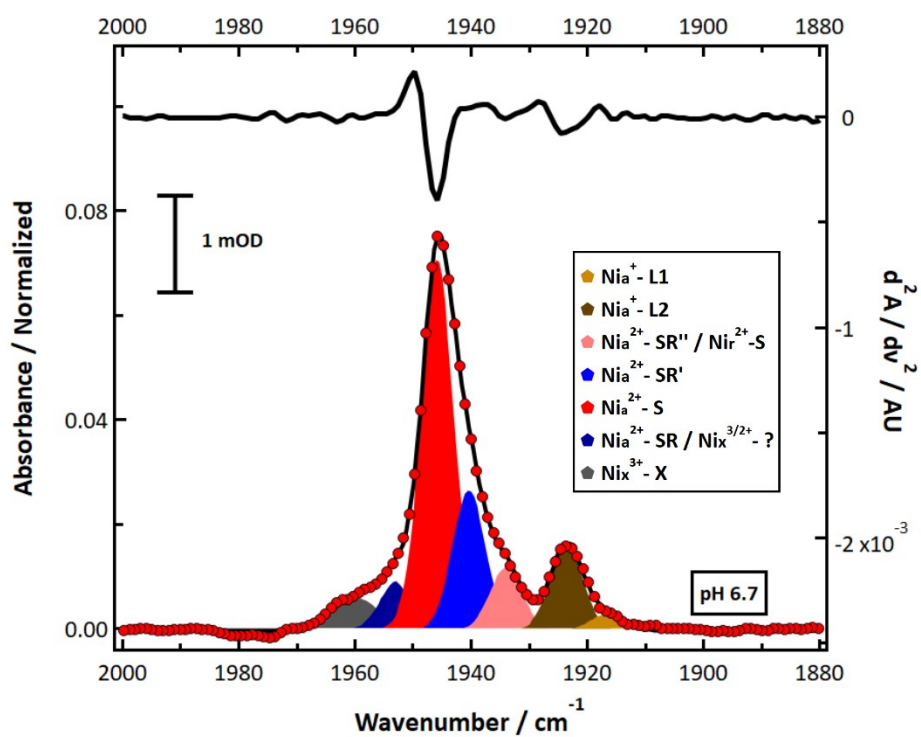


Figure S15: Normalized FTIR spectrum and the second derivative spectrum in the ν_{CO} region of the R355K SH1 pH 6.7 sample prepared under $\sim 4 \pm 1\%$ hydrogen in 25 mM MOPS buffer.

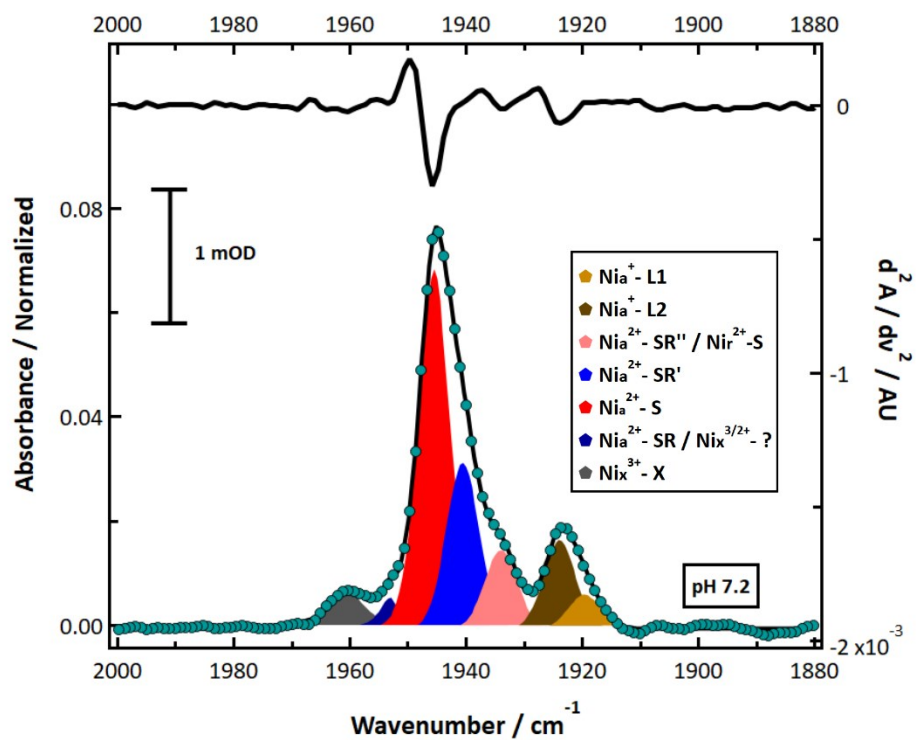


Figure S16: Normalized FTIR spectrum and the second derivative spectrum in the ν_{CO} region of the R355K SH1 pH 7.2 sample prepared under 4 +/- 1% hydrogen. The spectra plotted here are from exact same data that is the dark spectrum in **Figure S9** and **Figure S10** and in **Figure 4a**.

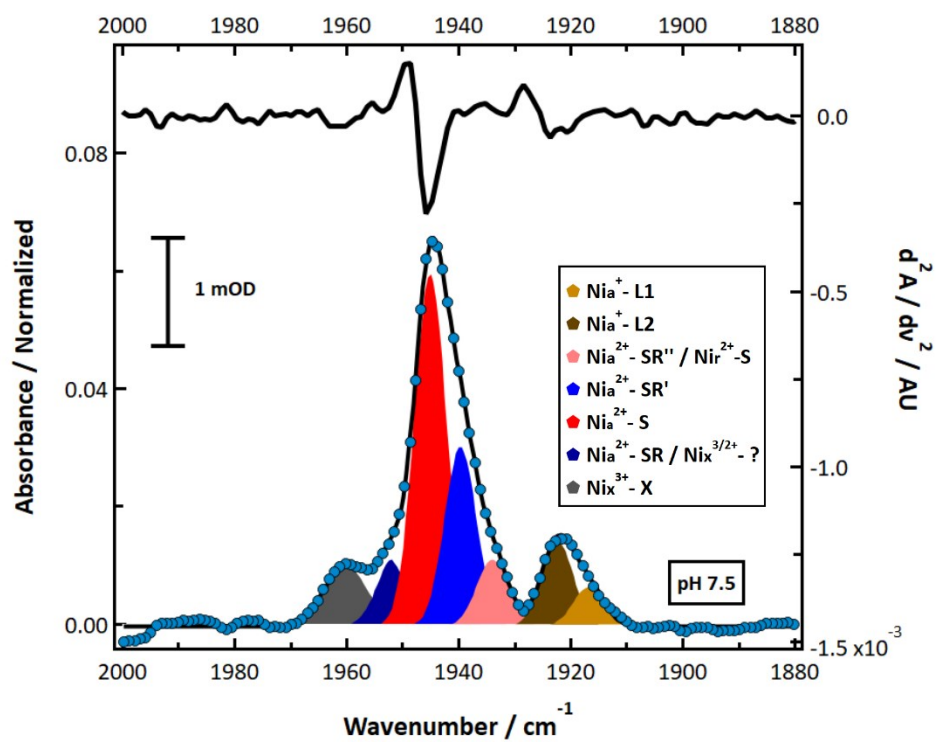


Figure S17: Normalized FTIR spectrum and the second derivative spectrum in the ν_{CO} region of the R355K SH1 pH 7.5 sample prepared under $\sim 4 \pm 1\%$ hydrogen in 50 mM Tris buffer.

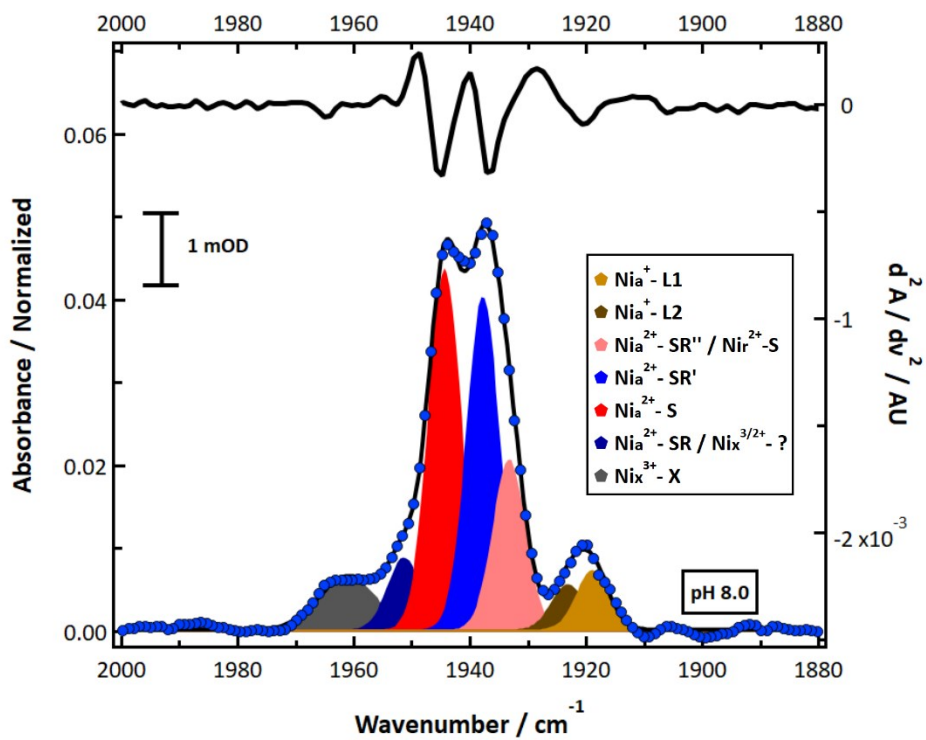


Figure S18: Normalized FTIR spectrum and the second derivative spectrum in the ν_{CO} region of the R355K SH1 pH 8.0 sample prepared under $\sim 4 \pm 1\%$ hydrogen in 50 mM HEPES buffer.

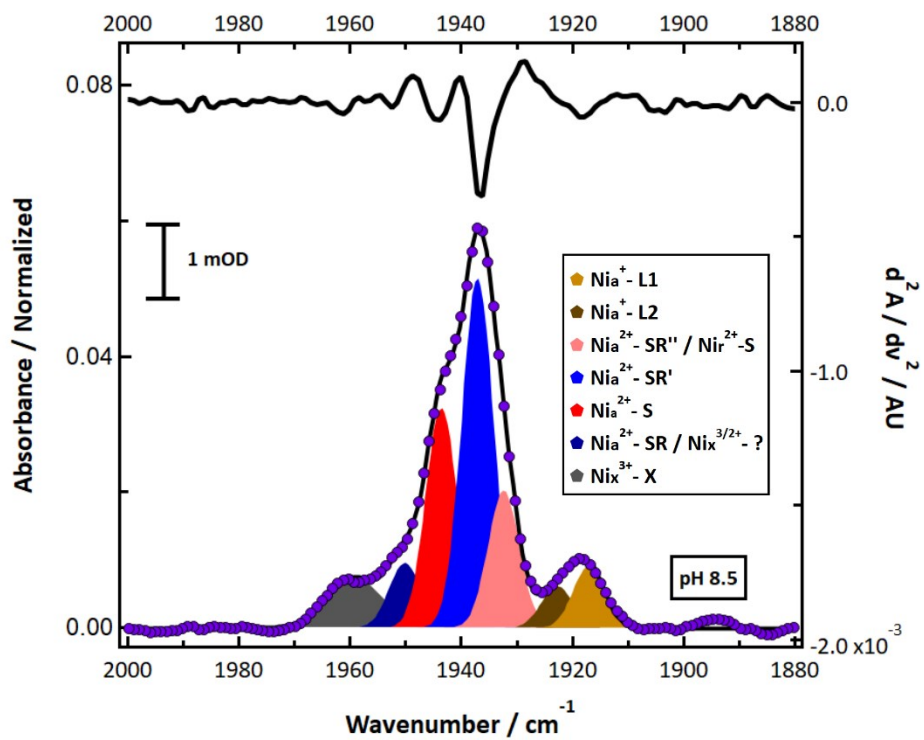


Figure S19: Normalized FTIR spectrum and the second derivative spectrum in the ν_{CO} region of the R355K SH1 pH 8.5 sample prepared under $\sim 4 \pm 1\%$ hydrogen in 50 mM HEPPS buffer.

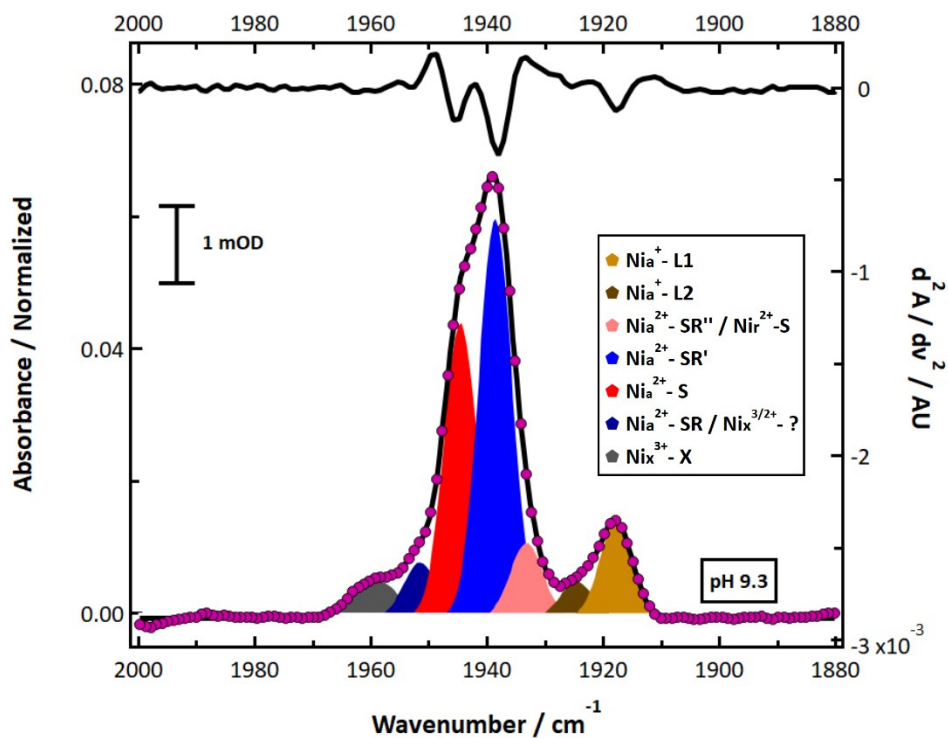


Figure S20: Normalized FTIR spectrum and the second derivative spectrum in the ν_{CO} region of the R355K SH1 pH 9.3 sample prepared under $\sim 4 \pm 1\%$ hydrogen in 25 mM glycine buffer.

Table S10: Peak positions from Voigt fits of the pH dependent spectra from pH 6.7 – 9.3. Errors are provided in parenthesis. Units are wavenumbers (cm^{-1}). The differences between the various forms of the $\text{Ni}_a^{2+}\text{-SR}$ states are not known, but are believed to differ by a protonation state of at least one amino acid residue near the [NiFe] active site.^{39, 40}

pH	$\text{Ni}_a^+\text{-L1}$	$\text{Ni}_a^+\text{-L2}$	$\text{Ni}_r^{2+}\text{-SI} /$	$\text{Ni}_a^{2+}\text{-SR}'$	$\text{Ni}_a^{2+}\text{-S}$	$\text{Ni}_x^{2+}\text{-?} /$	$\text{Ni}_x^{3+}\text{-X}$
----	---------------------------	---------------------------	--------------------------------	-------------------------------	-----------------------------	-------------------------------	-----------------------------

			$\text{Ni}_a^{2+}\text{-SR}''$			$\text{Ni}_a^{2+}\text{-SR}$	
6.7	1916.8 (0.5)	1923.6 (0.098)	1934 (0.19)	1940.4 (0.2)	1945.8 (0.06)	1953.1 (0.3)	1960 (0.7)
7.2	1919.6 (0.8)	1923.9 (0.3)	1934 (0.15)	1940.6 (0.2)	1945.5 (0.08)	1953.2 (0.16)	1960.3 (0.17)
7.5	1916.8 (0.6)	1922.4 (0.3)	1934 (0.4)	1939.7 (0.4)	1945.1 (0.14)	1952.1 (0.3)	1960.2 (0.3)
8.0	1918.9 (0.8)	1923.2 (1.14)	1933.3 (0.4)	1937.8 (0.3)	1944.4 (0.07)	1951.4 (0.2)	1961.1 (0.3)
8.5	1917.1 (0.3)	1922.8 (0.6)	1932.4 (0.4)	1937.1 (0.2)	1943.6 (0.11)	1950.2 (0.3)	1959.2 (0.4)
9.3	1917.8 (0.08)	1924.6 (0.2)	1933.2 (0.3)	1938.6 (0.08)	1944.6 (0.06)	1951.6 (0.2)	1959.3 (0.3)

Table S11: Integrated peak areas at FWHM for the R355K pH dependent spectra (prior to scaling for oscillator strength differences).

pH	$\text{Ni}_a^{+}\text{-L1}$	$\text{Ni}_a^{+}\text{-L2}$	$\text{Ni}_r^{2+}\text{-SI} / \text{Ni}_a^{2+}\text{-SR}''$	$\text{Ni}_a^{2+}\text{-SR}'$	$\text{Ni}_a^{2+}\text{-S}$	$\text{Ni}_x^{2+}\text{-?} / \text{Ni}_a^{2+}\text{-SR}$	$\text{Ni}_x^{3+}\text{-X}$
6.7	0.011	0.061	0.044	0.0100	0.257	0.034	0.034
7.2	0.024	0.062	0.056	0.117	0.247	0.018	0.040
7.5	0.025	0.053	0.042	0.113	0.220	0.041	0.052
8.0	0.026	0.020	0.076	0.148	0.160	0.032	0.042
8.5	0.033	0.023	0.075	0.190	0.119	0.035	0.048
9.3	0.053	0.020	0.042	0.222	0.164	0.031	0.030

Table S12: Integrated peak areas at FWHM for the R355K pH dependent spectra scaled for oscillator strength differences³⁷ relative to the $\text{Ni}_a^{+}\text{-L}(1/2)$ ν_{CO} region.

pH	$\text{Ni}_a^{+}\text{-L1}$	$\text{Ni}_a^{+}\text{-L2}$	$\text{Ni}_r^{2+}\text{-SI} / \text{Ni}_a^{2+}\text{-SR}''$	$\text{Ni}_a^{2+}\text{-SR}'$	$\text{Ni}_a^{2+}\text{-S}$	$\text{Ni}_x^{2+}\text{-?} / \text{Ni}_a^{2+}\text{-SR}$	$\text{Ni}_x^{3+}\text{-X}$
6.7	0.011	0.061	0.046	0.103	0.280	0.038	0.040
7.2	0.024	0.062	0.058	0.122	0.268	0.022	0.048
7.5	0.025	0.053	0.044	0.117	0.240	0.046	0.062
8.0	0.026	0.020	0.079	0.154	0.174	0.036	0.050
8.5	0.033	0.023	0.078	0.198	0.130	0.040	0.057
9.3	0.053	0.020	0.043	0.232	0.179	0.035	0.036

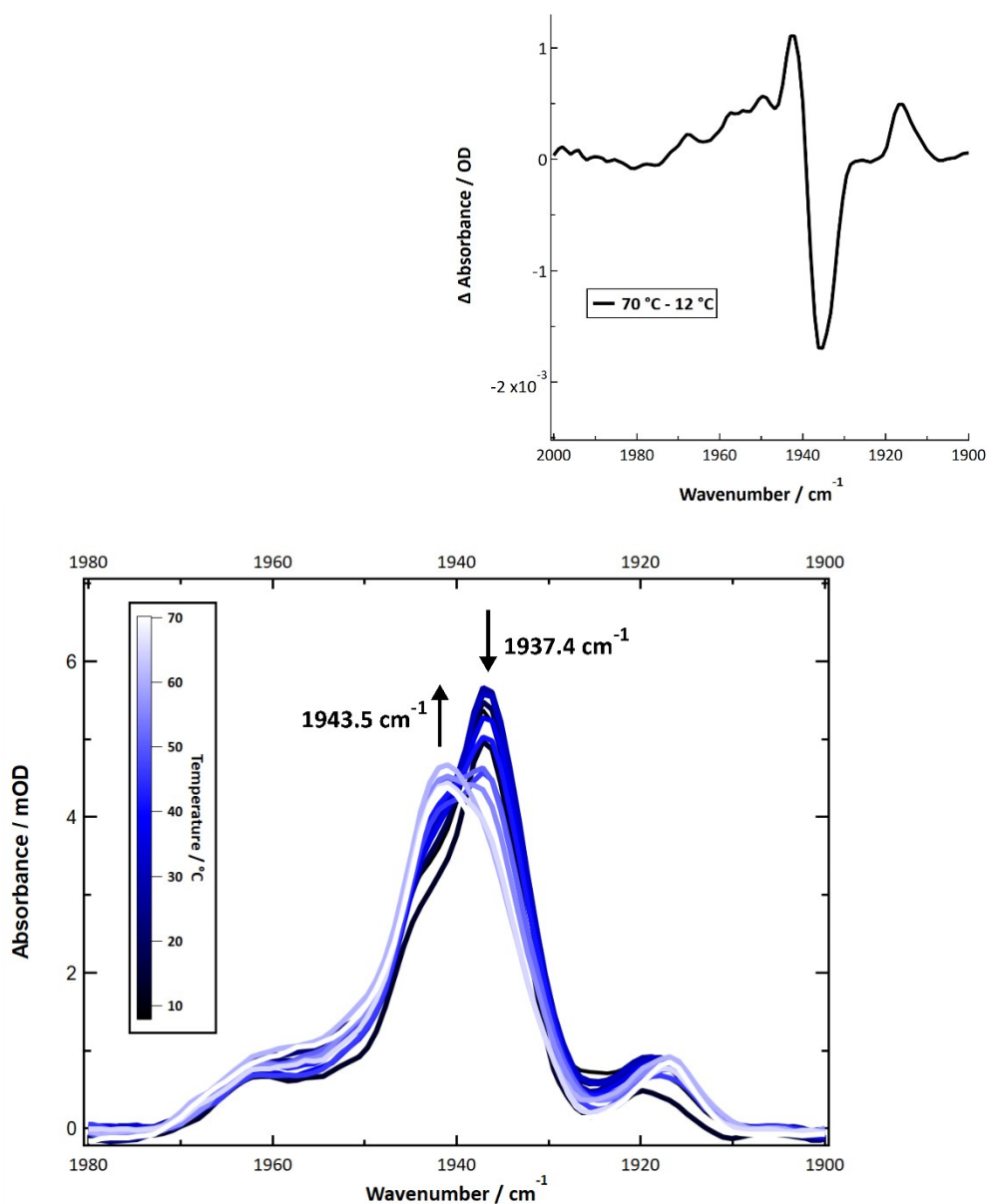


Figure S21: FTIR spectra of R355K SH1 at pH = 8.5 as a function of temperature (8 °C – 70 °C). The T = 21 °C data point is the same data used in the pH dependent FTIR analysis. The original cell atmosphere was ~ 4 % H₂. Hydrogen processing and/or hydrogen loss from the cell resulted in notable enzyme auto-oxidation, with the most reduced state of the enzyme (Ni_a²⁺-SR' ; 1937.4 cm⁻¹) decreasing in intensity, and the oxidized form of the enzyme (one or both of Ni_a²⁺-S / Ni_r²⁺-S(II) ; 1943.5 cm⁻¹) increasing in intensity. This is further verification of which major state in the spectrum is more reduced and which major state is more oxidized. Inset: difference spectrum of 70 °C versus 12 °C, which clearly shows the bleach of the 1937.4 cm⁻¹ feature and the growth of the 1943.5 cm⁻¹ feature.

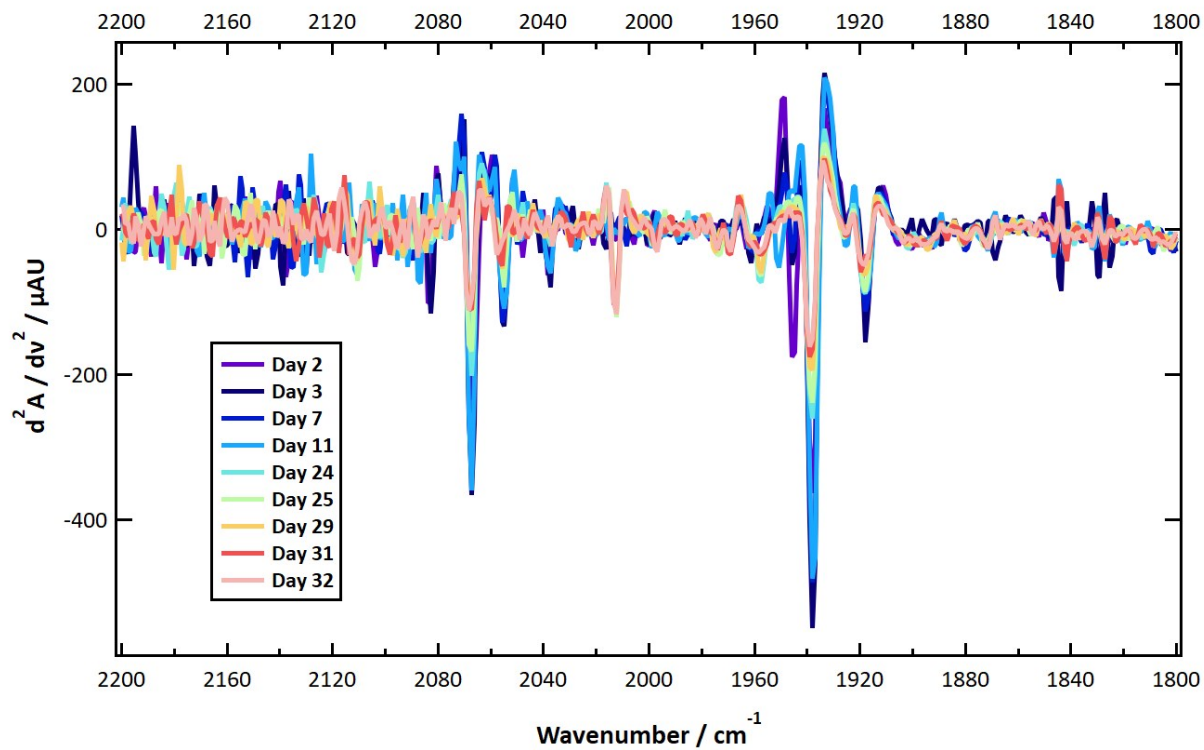


Figure S22: Second derivative spectra of the R355K pH = 9.3 sample over the course of 32 days.

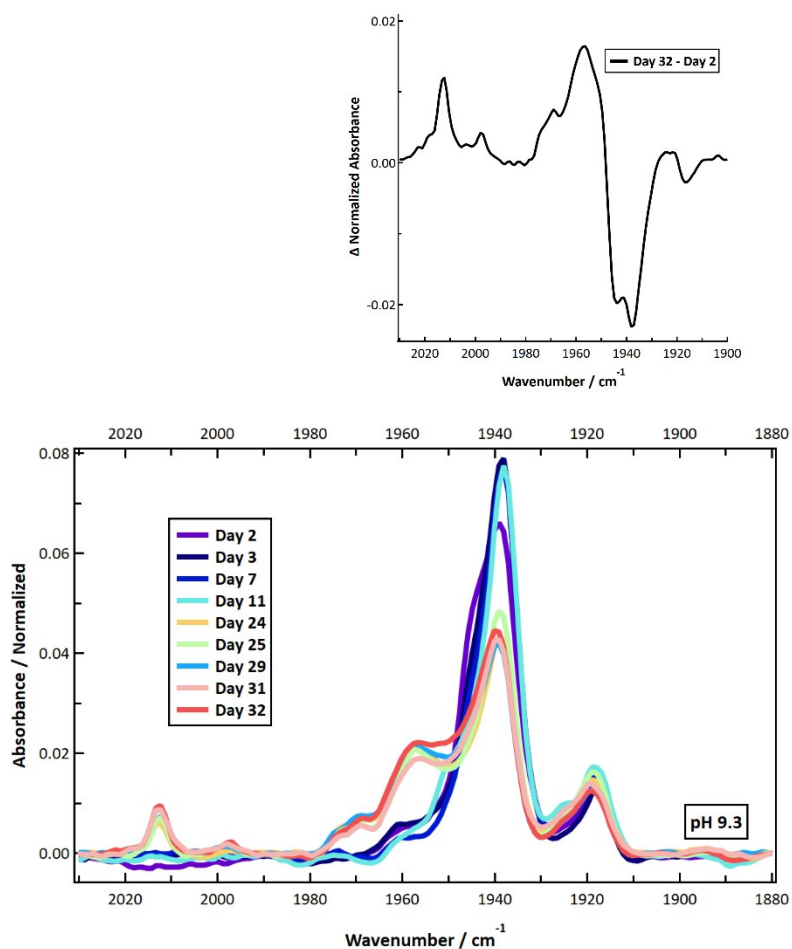


Figure S23: Absorbance FTIR spectra of the R355K pH 9.3 day dependent FTIR spectra as observed over the course of 32 days. Inset: difference spectrum of day 32 versus day 2 (subtraction of the normalized spectra), which shows clear absorbance decreases near 1917, 1938, and 1944 cm^{-1} and absorbance increases near 1958, 1969, 1998, and 2012 cm^{-1} .

Table S13: Area under the curve (AOC) used for normalization of FTIR data for each pH = 9.3 spectrum after baseline correction and an offset to 0.0 O.D. at 1880 cm^{-1} .

Day	AOC, 1880 – 2000 cm^{-1} (Days 2 –
-----	---

11)	
AOC, 1880 – 2030, (Days 24 – 32)	
2*	0.0871
3	0.0810
7	0.0730
11	0.0670
24	0.0762
25	0.0611
29	0.0649
31	0.0596
32	0.0550

*identical data to **Table S6**; data was taken within 16 - 18 hours of sample preparation; an extreme amount of water vapor was initially observed that unfortunately necessitated overnight purging in the external FTIR box.

Table S14: Peak positions from Voigt fits of the day dependent spectra for pH = 9.3 of R355K. Units are wavenumbers (cm⁻¹). Errors are provided in parenthesis.

Day	Ni _a ⁺ -L1	Ni _a ⁺ -L2	Ni _i ²⁺ -SI / Ni _a ²⁺ -SR''	Ni _a ²⁺ -SR'	Ni _a ²⁺ -S	Ni _x ²⁺ - ? / Ni _a ²⁺ -SR	Ni _x -X2	Ni _x -X3	Ni _x -X4	Ni _x -X5
Day 2*	1917.8 (0.08)	1924.6 (0.2)	1933.2 (0.3)	1938.6 (0.08)	1944.6 (0.06)	1951.6 (0.2)	1959.3 (0.3)	-	-	-
Day 3	1918.0 (0.12)	1924.5 (0.5)	1932.9 (0.6)	1938.2 (0.09)	1944.3 (0.11)	1950.7 (0.4)	1958.8 (0.5)	-	-	-
Day 7	1918.0 (0.08)	1925.1 (0.2)	1932.8 (0.5)	1938.1 (0.07)	1944.3 (0.2)	1950.4 (0.5)	1958.8 (0.8)	-	-	-
Day 11	1918.0 (0.09)	1925.7 (0.2)	1935.9 (0.9)	1938.4 (0.3)	1943.9 (0.4)	1950.1 (0.3)	1958.0 (0.4)	-	-	-
Day 24	1918.2 (0.11)	1924.8 (0.3)	1932.1 (0.7)	1938.4 (0.13)	1944 (0.3)	1950.5 (0.4)	1958.3 (0.17)	1970 (0.16)	n.d.	2012.4 (0.10)
Day 25	1918.4 (0.06)	1925.3 (0.14)	1936 (0.7)	1939.2 (0.3)	1945 (0.3)	1951.5 (0.4)	1958.4 (0.2)	1970.3 (0.15)	1998.0 (0.3)	2012.5 (0.06)
Day 29	1918.3 (0.13)	1924 (0.3)	1931.1 (0.4)	1938.6 (0.11)	1943.8 (0.3)	1949.9 (0.3)	1958.2 (0.11)	1970.0 (0.10)	1998.5 (0.3)	2012.6 (0.05)
Day 31	1918.3 (0.14)	1924.7 (0.3)	1932.4 (0.6)	1938.8 (0.18)	1944.2 (0.5)	1949.5 (0.8)	1957.2 (0.3)	1970.7 (0.5)	n.d.	2012.6 (0.08)
Day 32	1918.6 (0.11)	1925 (0.3)	1933.7 (1.11)	1939 (0.2)	1944.3 (0.4)	1950.8 (0.3)	1959 (0.16)	1969.7 (0.17)	1997.4 (0.2)	2012.7 (0.06)

*identical data to **Table S10**.

n.d. : not determined

5. Fourier Transform Infrared Spectroscopy Incubated Samples Incubated Under a CO Atmosphere

FTIR absorbance spectra for samples incubated with CO were obtained by subtracting a given reference spectrum from the sample spectrum ($\Delta A = -\log(I_{\text{enzyme}}/I_{\text{buffer}})$). A spline baseline correction was applied between 1965 – 1910 cm^{-1} ; 1980 – 2030 cm^{-1} ; and 2100 – 2200 cm^{-1} for the native and E17Q samples, and between 1985 – 1910 cm^{-1} ; 1980 – 2000 cm^{-1} ; and 2110 – 2200 cm^{-1} for the R355K sample (to avoid overlap with the ν_{CO} and ν_{CN} peaks observed in both second derivative spectra and absorbance spectra, we could not utilize the entire 1980 – 2030 cm^{-1} region with R355K SH1). The second derivative spectra are plotted together in **Figure S24**.

The native and R355K spectra were fit to the ν_{CO} and ν_{CN} region using **equation 1**. The data were significantly noisy in the region $> 2050 \text{ cm}^{-1}$ for the E17Q enzyme, and only the endogenous ν_{CO} region was fit for E17Q. The peak widths for native SH1 were constrained $\leq 5 \text{ cm}^{-1}$ and for E17Q SH1 were constrained $\leq 6 \text{ cm}^{-1}$. For R355K SH1, peak widths were used as described above for the pH dependent spectra, and presumable exogenous ν_{CO} peaks were constrained $\leq 5 \text{ cm}^{-1}$. The individual fits and corresponding second derivative spectrum for each CO inhibited sample are provided in **Figure S25 – S27**. The frequencies corresponding to endogenous CO are presented in **Table S14**, and the frequencies corresponding to exogenous CO are presented in **Table S15**.

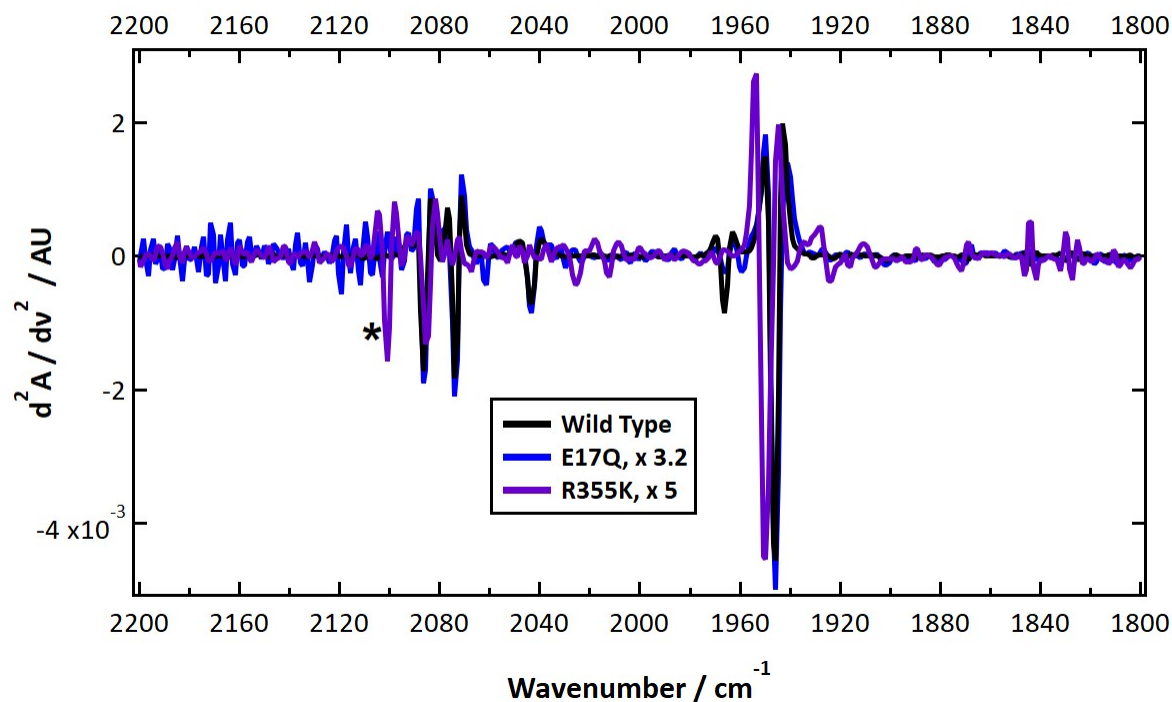


Figure S24: Second derivative spectra of WT, E17Q, and R355K SH1 after being purged with CO at pH = 8.0. The E17Q and R355K spectra have been scaled for better visual comparison to the native enzyme. The asterisk marks an unusually high frequency CN peak relative to native and E17Q SH1 incubated with CO, as well as typical CN frequencies observed in native and E17Q SH1 under a nitrogen and/or hydrogen/nitrogen mixed atmosphere.^{2, 12, 36}

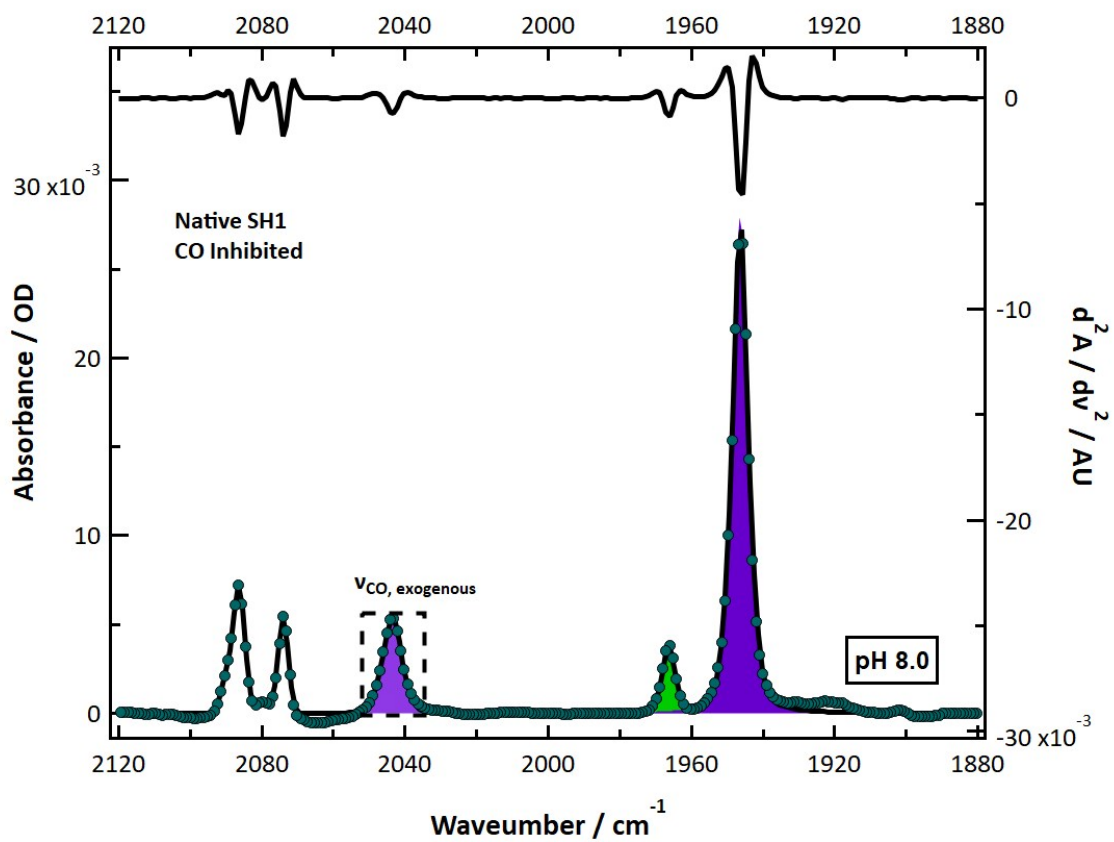


Figure S25: FTIR spectrum and the corresponding second derivative spectrum of WT SH1 under a CO atmosphere at pH 8.0 in 50 mM HEPES buffer. Residual $\text{Ni}_a^{3+}\text{-C}$ was present near 1666 cm^{-1} .

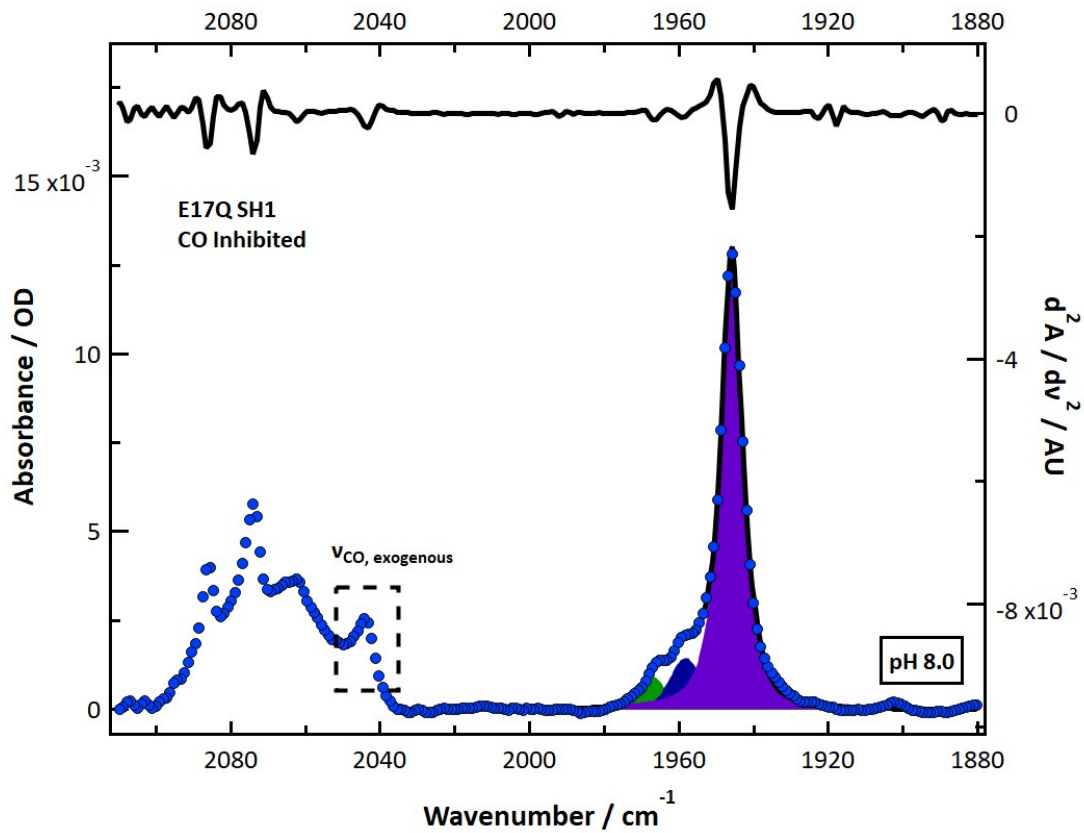


Figure S26: FTIR spectrum and the corresponding second derivative spectrum of E17Q SH1 under a CO atmosphere at pH 8.0 in 50 mM HEPPS buffer. Residual Ni_a-C was present near 1967 cm⁻¹. An unknown species was near 1958.2 cm⁻¹, which may be an inactive state.

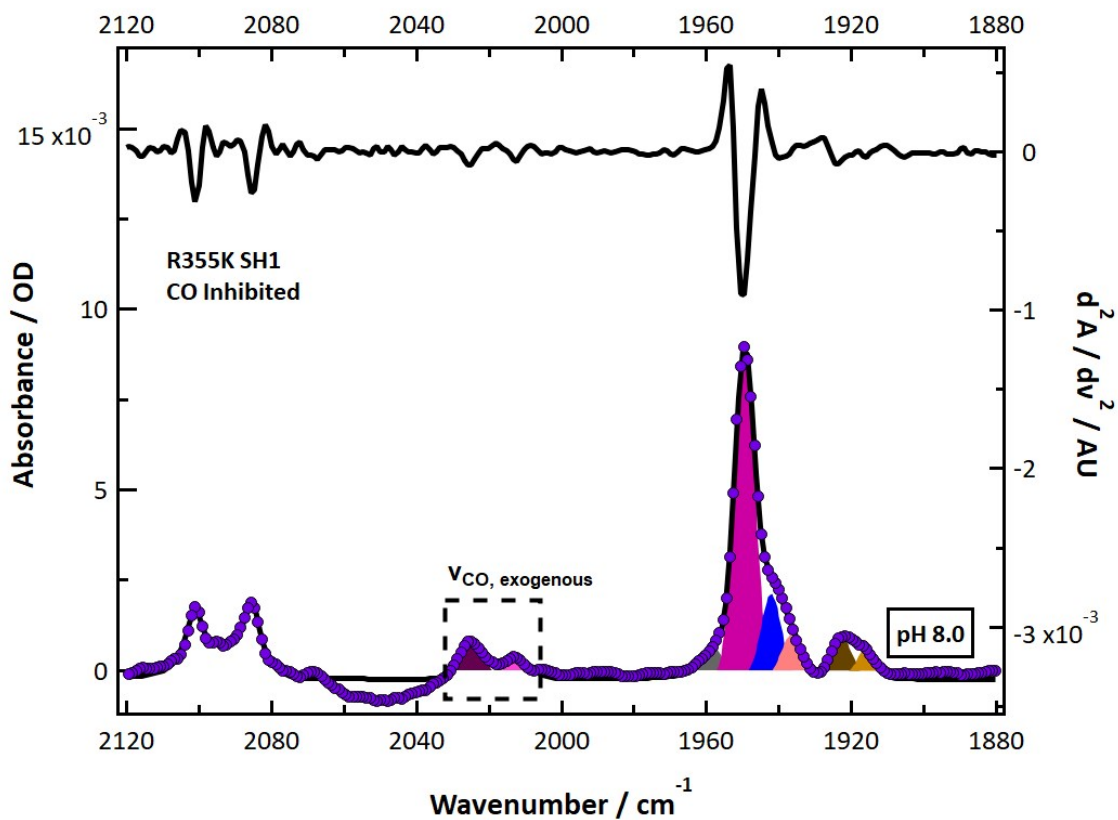


Figure S27: FTIR spectrum and the corresponding second derivative spectrum of R355K enzyme under a CO atmosphere at pH 8.0 in 50 mM HEPPS buffer. The state near 1950 cm^{-1} (color coded light purple) does not clearly correspond to other states we observed for R355K that are discussed in this manuscript, and is believed to represent the CO bound to the active site nickel in R355K SH1.

Table S15: Endogenous CO frequencies observed for WT, R355K, and E17Q SH1.

Enzyme	Ni _a ⁺ -L1	Ni _a ⁺ -L2	Ni ²⁺ -X	Ni ²⁺ -X2	Ni ²⁺ -CO M-CO	Ni ²⁺ -X3	Ni _a ³⁺ -C*
Wild Type	-	-	-	-	1946.4 (0.014)	-	1966.4 (0.095)
R355K	1916.3 (0.7)	1922.7 (0.5)	1936.8 (1.2)	1942.2 (0.8)	1949.5 (0.08)	1958.3 (0.5)	-
E17Q	-	-	-	-	1945.9 (0.02)	1958.2 (0.4)	1966.7 (0.5)

* Varying amounts very minor amounts to no detectable Ni_a³⁺-C have been observed between various preparations.

Table S16: Exogenous CO frequencies observed for WT, R355K, and E17Q SH1.

Enzyme	Ni-CO(1)	Ni-CO(2)	Ni ²⁺ -CO
Wild Type	-	-	2043.6 (0.08)
R355K	2012.9 (1.03)	2024.9 (0.5)	-
E17Q	-	-	~ 2044*

*visually estimated

6. Temperature Methyl Viologen Oxidation Reduction of Native and R355K Pf SH1 under 5% H₂ monitored via UV-Vis Spectroscopy

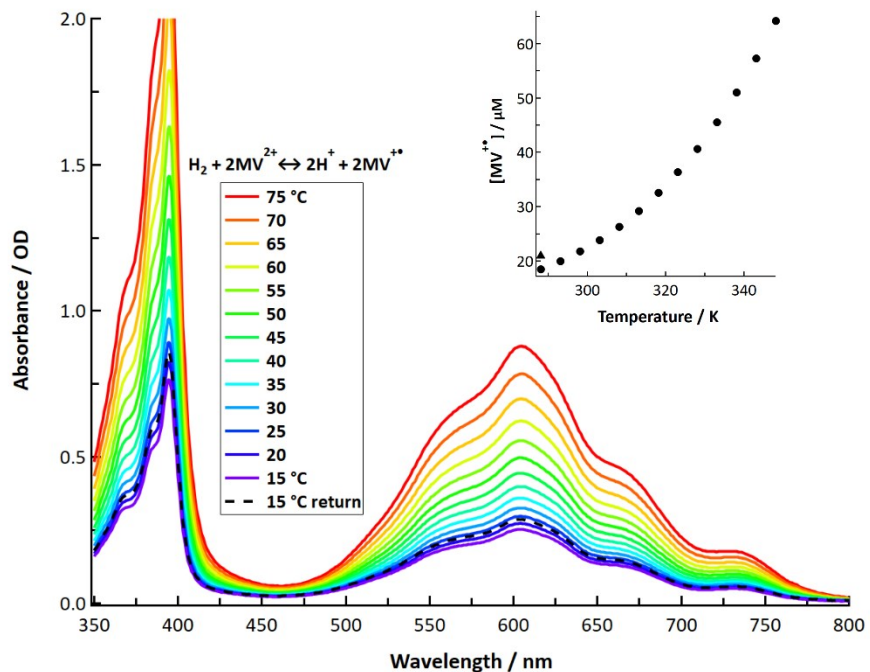


Figure S28: Temperature dependent equilibration of native SH1 with 5% hydrogen and an external electron donor/acceptor, methyl viologen.¹⁰ This is a simple demonstration that SH1 undergoes reversible redox behavior over a wide temperature range because the equilibration with the hydrogen and methyl viologen was reversible within reasonable error. Conditions: pH = 7.2, 50 mM potassium phosphate buffer; 50 nM native SH1; 330 μM methyl viologen; and an ~5 % H₂ and 95% N₂ gas composition. Inset: The concentration of methyl viologen radical observed at a given temperature assuming an extinction coefficient of 13,700 cm⁻¹M⁻¹ at 605 nm.⁴¹

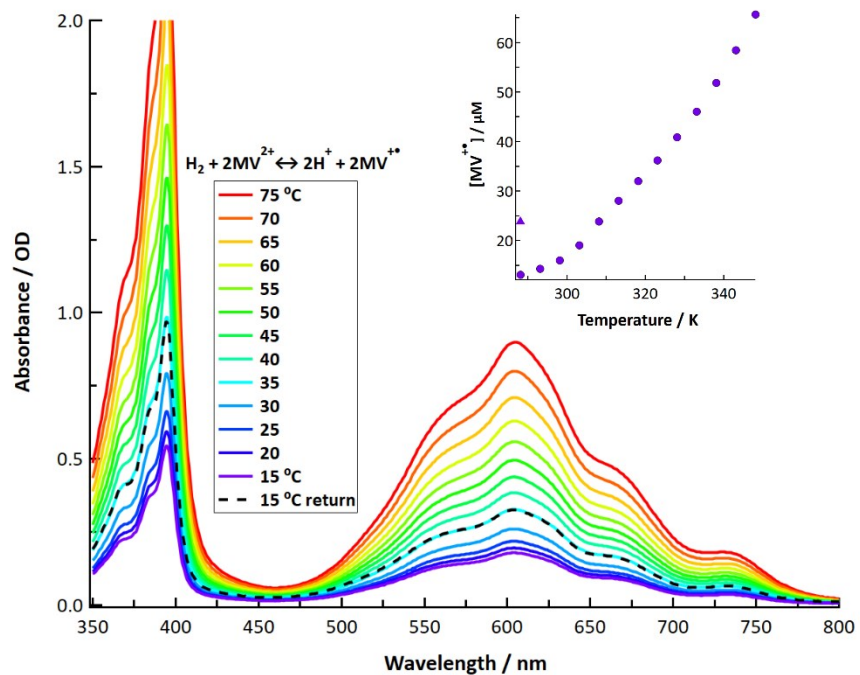


Figure S29: Temperature dependent equilibration of R355K with 5% hydrogen and an external electron donor/acceptor, methyl viologen. The procedure and conditions were identical to those for the data collected in **Figure S23**. Despite waiting > 25 minutes upon returning to 15 °C as opposed to the 7 minute equilibration times for the temperature ramp, we were unable to see the absorbance spectrum return any closer to the starting value. Conditions: pH = 7.2, 50 mM potassium phosphate buffer; 50 nM R355K SH1; 330 μ M methyl viologen; and an ~5 % H_2 and 95% N_2 gas composition. Inset: The concentration of methyl viologen radical observed at a given temperature assuming an extinction coefficient of $13,700 \text{ cm}^{-1}\text{M}^{-1}$ at 605 nm.⁴¹

7. Additional Analysis: The pK_a of Lysine (K355) in the Ni_a^{3+} -C State is Probably not Perturbed from Its Solution Value

Although it appears the Ni_a^{3+} -C \leftrightarrow Ni_a^{+} -L tautomeric equilibrium is shifted to favour Ni_a^{+} -L in R355K relative to native SH1, it is conceivable the lysine pK_a is lower than its solution value of 10.5,⁴² which would allow it to accept a proton. This would result in a Fe^{2+} -H- Ni^{3+} (-NH₂) \leftrightarrow Fe^{2+} - Ni^{+} + (-NH₃) equilibrium (that is, Ni_a^{3+} -C \leftrightarrow new Ni_a^{+} state, which would essentially compete with the formation Ni_a^{+} -L). C418 would not be protonated. The resultant Ni_a^{+} state would have a ν_{CO} frequency redshifted by $> 10\text{ cm}^{-1}$ relative to Ni_a^{+} -L because of the increased electron density at the active site in the absence of C418 protonation,^{40, 43} and the lower energy ν_{CO} would have a greater oscillator strength.³⁷ We found no evidence of such a species (see the second derivative spectra in **Figure S10** and **S13**). This suggests lysine retains a pK_a value near 10.5 in the Ni_a^{3+} -C (and probably Ni_a^{+} -L states), and that the proton predominantly migrates to C418.

8. Additional Analysis and Discussion of the CN Features and Exogenous CO Binding Results

Native Enzyme CO Inhibited Features and CO Inhibited Native and E17Q SH1

Prior results in our laboratory have shown that the Ni_a^{2+} -S state in *Pf* SH1 has ν_{CN} features at ~ 2091 and 2080 cm^{-1} ,^{1,36} which is in good agreement with $\Delta\nu_{CN, \text{symm}} - \Delta\nu_{CN, \text{asymm}} \sim 10 - 15\text{ cm}^{-1}$ in other [NiFe]-hydrogenases^{39, 44-47} (this is, of course, not always the case³¹). The endogenous CO band is $\sim 1951\text{ cm}^{-1}$. When incubated under CO, we found the enzyme to primarily adopt a CO inhibited state with an endogenous CO band redshifted from 1951 cm^{-1} in the Ni_a^{2+} -S state to 1946 cm^{-1} in the CO inhibited state. The CN bands also underwent small redshifts. As shown in **Table S14**, such behaviour is consistent with most hydrogenases in the Ni_a^{2+} -SCO state. The endogenous CO band appeared near 2044 cm^{-1} . As shown in **Table S15**, this is a reasonable endogenous CO peak position; although comparison to the other CO inhibited hydrogenases indicate somewhat stronger CO binding in SH1 (the band is $\sim 10\text{ cm}^{-1}$ lower in energy than most endogenous bands in **Table S15**). Despite the spectra in the endogenous CO region and CN region being noisier, CO inhibited E17Q also did display nearly identical features.

Identification R355K SH1 CN Features at pH = 7.2 and Under a CO Atmosphere

Regarding R355K, determining CN bands from the pH dependent infrared spectra and photochemical reduction proved to be incredibly challenging. This is not surprising, because each absorbance spectra has at least 5 clear bands, which means that there are at least 10 CN vibrations within the $\sim 2030 - 2100\text{ cm}^{-1}$ region. Using difference spectra from the pH = 7.2 photochemical reduction in the CN region, the clear induced absorbance features near 2070 and 2054 cm^{-1} were readily assigned to Ni_a^{2+} -SR' in accord with the strong induced absorbance of this state in the CO region. The clear bleach near 2084 cm^{-1} was able to be assigned to Ni_a^{2+} -S. The other Ni_a^{2+} -S CN feature either appears between $\sim 2090 - 2100\text{ cm}^{-1}$ or 2064 cm^{-1} (**Figure S12**). The pH = 6.7 sample, which primarily adopts the Ni_a^{2+} -S state over Ni_a^{2+} -SR', has a feature near 2064 cm^{-1} (the feature can be distinguished from the $\sim 2070\text{ cm}^{-1}$ Ni_a^{2+} -SR' peak in the second derivative spectra, which is an important point to make because of the weak signals in the CN region and noisy baseline). We thus favour the additional CN peak being 2064 cm^{-1} .

When R355K was incubated with CO, the behaviour was significantly different than native and E17Q SH1. The enzyme still displayed a broad distribution of states, which was surprising, yet reproducible. The main ν_{CO} peak was different from what we observed in the pH dependent samples and ascribed to the CO inhibited state ($\sim 1950\text{ cm}^{-1}$), and the two clear major CN peaks (~ 2101 and 2085 cm^{-1}) were assumed to correspond to this CO feature. The CO feature and at least one of the CN features are blueshifted compared to the native Ni_a^{2+} -S state (**Table S14**).

The peaks from external CO appeared near 2025 and 2013 cm^{-1} , which are significantly blueshifted from the typical exogenous ν_{CO} region in [NiFe]-hydrogenases (**Table S15**).

Table S17: Endogenous CO and CN Peak Position Comparisons of Ni_a²⁺-S vs Ni_a²⁺-SCO for various hydrogenase enzymes. Units are cm⁻¹. Peaks are ordered as: ν_{CO} , $\nu_{CN, asymm}$, $\nu_{CN, symm}$. Each enzyme group and subgroup is also provided.^{17, 18}

Enzyme Source / State	Group	Ni _a ²⁺ -S	Ni _a ²⁺ -SCO	Differences (Ni _a ²⁺ -S - Ni _a ²⁺ -SCO)	Ref.
<i>Desulfovibrio fructosovrans</i> *	1b	1933 2074, 2087	1931 2069, 2084	2 5, 3	47, 48
<i>D. gigas</i>	1a	1934 2075, 2086	1932 2070, 2083	2 5, 3	47
<i>Allochrochmatium vinosum</i>	1e	1931 2073, 2084	1929 2069, 2082	2 4, 2	47, 49
<i>Methanosarcina barkeri</i> MS	3a	1945 2065, 2080	1936, 2073, 2086	9 -8, -6	50
<i>Aquifex aeolicus</i> hydrogenase-1	1d	1927 2077, 2086	1925 2072, 2082	2 5, 4	46
<i>D. vulgaris</i> Miyazaki F*	1a	1943 2074, 2086	1941 2071, 2084	2 3, 2	51
<i>Pyrococcus furiosus</i> SH1, native	3b	1951 2080, 2091	1946 2074 (0.09), 2086.5 (0.17)	5 6, 4.5	³⁶ and this work
<i>Pyrococcus furiosus</i> SH1, R355K	""	1945 2084	1949.5 2085.4 (0.7), 2101 (0.5)	-4.5 -	this work

Table S18: Exogenous CO Peak Position Comparisons of Ni_a²⁺-S vs Ni_a²⁺-SCO for various hydrogenase enzymes. Units are cm⁻¹.

Enzyme Source / State	Ni _a ²⁺ -SCO	Ref.
<i>Desulfovibrio fructosovrans</i>	2055	47, 48
<i>Desulfovibrio gigas</i>	2056	47
<i>Allochrochmatium vinosum</i>	2060	47, 49
<i>Methanosarcina barkeri</i> MS	2048	50
<i>Aquifex aeolicus</i> hydrogenase-1	2066	46
<i>D. vulgaris</i> Miyazaki F*	2056	51
<i>Pyrococcus furiosus</i> SH1, native	2044	this work
<i>Pyrococcus furiosus</i> SH1, R355K	2024.9 (0.5), 2012.9 (1.03)	this work

* the Ni-SCO_{red} state has slightly lower energy values for the CO inhibited state by ~ 1 - 3 cm⁻¹ relative to Ni-SCO_{ox}, which is believed to be related primarily to the oxidation state of the proximal iron-sulfur cluster at a given pH.

** we could only confidently determine one ν_{CN} value; the other band would show up near 2094 or 2064 cm⁻¹ as discussed above.

Supplemental Information References

1. S. K. Chandrayan, C.-H. Wu, P. M. McTernan and M. W. W. Adams, *Protein Expres. Purif.*, 2015, **107**, 90-94.
2. B. L. Greene, G. E. Vansuch, C.-H. Wu, M. W. W. Adams and R. B. Dyer, *J. Am. Chem. Soc.*, 2016, **138**, 13013-13021.
3. C.-H. Wu, C. A. Ponir, D. K. Haja and M. W. W. Adams, *Protein Eng., Des. Sel.*, 2018, **31**, 337-344.
4. B. C. Chica, Ph.D. Thesis, Emory University, 2017.
5. B. Chica, C.-H. Wu, Y. Liu, M. W. W. Adams, T. Lian and R. B. Dyer, *Energy Environ. Sci.*, 2017, **10**, 2245-2255.
6. R. F. Homer and T. E. Tomlinson, *J. Chem. Soc.*, 1960, **0**, 2498-2503.
7. S. G. Mayhew, *Eur. J. Biochem.*, 1978, **85**, 535-547.
8. C. Zhao, E. N. Glass, B. Chica, D. G. Musaev, J. M. Sumliner, R. B. Dyer, T. Lian and C. L. Hill, *J. Am. Chem. Soc.*, 2014, **136**, 12085-12091.
9. J. R. Ferraro, K. Nakamoto and C. W. Brown, *Introductory Raman Spectroscopy*, Academic Press, Cambridge, MA, 2 edn., 2002.
10. B. L. Greene, Ph.D. Thesis, Emory University, 2015.
11. Y. Kawahara-Nakagawa, K. Nishikawa, S. Nakashima, S. Inoue, T. Ohta, T. Ogura, Y. Shigeta, K. Fukutani, T. Yagi and Y. Higuchi, *Protein Sci.*, 2019, **28**, 663-670.
12. B. L. Greene, C. H. Wu, G. E. Vansuch, M. W. Adams and R. B. Dyer, *Biochemistry*, 2016, **55**, 1813-1825.
13. S. Stoll and A. Schweiger, *J. Magn. Reson.*, 2006, **178**, 42-55.
14. P. J. Silva, B. De Castro and W. R. Hagen, *J. Biol. Inorg. Chem.*, 1999, **4**, 284-291.
15. W. Lubitz, E. Reijerse and M. van Gatsel, *Chem. Rev.*, 2007, **107**, 4331-4365.
16. W. Lubitz, H. Ogata, O. Rudiger and E. Reijerse, *Chem. Rev.*, 2014, **114**, 4081-4148.
17. C. Greening, A. Biswas, C. R. Carere, C. J. Jackson, M. C. Taylor, M. B. Stott, G. M. Cook and S. E. Morales, *ISME J.*, 2016, **10**, 761-777.
18. Bioinformatics Research Centre, <https://services.birc.au.dk/hyddb/browser/>, (accessed May 2020).
19. J. W. Van der Zwaan, S. P. J. Albracht, R. D. Fontijn and E. C. Slater, *FEBS Lett.*, 1985, **179**, 271-277.
20. S. P. J. Albracht, A. Kroeger, J. W. Van der Zwaan, G. Unden, R. Boecher, H. Mell and R. D. Fontijn, *Biochim. Biophys. Acta, Protein Struct. Mol. Enzymol.*, 1986, **874**, 116-127.
21. J. P. Whitehead, R. J. Gurbiel, C. Bagyinka, B. M. Hoffman and M. J. Maroney, *J. Am. Chem. Soc.*, 1993, **115**, 5629-5635.
22. C. Fichtner, M. Van Gastel and W. Lubitz, *Phys. Chem. Chem. Phys.*, 2003, **5**, 5507-5513.
23. S. Foerster, M. Stein, M. Brecht, H. Ogata, Y. Higuchi and W. Lubitz, *J. Am. Chem. Soc.*, 2003, **125**, 83-93.
24. H. Tai, K. Nishikawa, S. Inoue, Y. Higuchi and S. Hirota, *J. Phys. Chem. B*, 2015, **119**, 13668-13674.
25. M. Medina, R. Williams, R. Cammack and E. C. Hatchikian, *J. Chem. Soc., Faraday Trans.*, 1994, **90**, 2921-2924.
26. M. Medina, E. C. Hatchikian and R. Cammack, *Biochim. Biophys. Acta, Bioenerg.*, 1996, **1275**, 227-236.
27. J. J. G. Moura, I. Moura, B. H. Huynh, H. J. Krueger, M. Teixeira, R. C. DuVarney, D. V. DerVartanian, A. V. Xavier, H. D. Peck, Jr. and J. LeGall, *Biochem. Biophys. Res. Commun.*, 1982, **108**, 1388-1393.
28. M.-E. Pandelia, P. Infossi, M. Stein, M.-T. Giudici-Orticoni and W. Lubitz, *Chem. Commun.*, 2012, **48**, 823-825.
29. M. M. Roessler, R. M. Evans, R. A. Davies, J. Harmer and F. A. Armstrong, *J. Am. Chem. Soc.*, 2012, **134**, 15581-15594.
30. B. J. Murphy, R. Hidalgo, M. M. Roessler, R. M. Evans, P. A. Ash, W. K. Myers, K. A. Vincent and F. A. Armstrong, *J. Am. Chem. Soc.*, 2015, **137**, 8484-8489.
31. M. Saggiu, I. Zebger, M. Ludwig, O. Lenz, B. Friedrich, P. Hildebrandt and F. Lenzian, *J. Biol. Chem.*, 2009, **284**, 16264-16276.
32. T. Buhrke, M. Brecht, W. Lubitz and B. Friedrich, *J. Biol. Inorg. Chem.*, 2002, **7**, 897-908.
33. M. Brecht, M. v. Gastel, T. Buhrke, F. Barbel and W. Lubitz, *J. Am. Chem. Soc.*, 2003, **125**, 13075-13083.
34. J. Lowenstein, L. Lauterbach, C. Teutloff, O. Lenz and R. Bittl, *J. Phys. Chem. B*, 2015, **119**, 13834-13841.
35. O. Schroeder, B. Bleijlevens, T. E. Jongh, Z. Chen, T. Li, J. Fischer, J. Foerster, C. G. Friedrich, K. A. Bagley, S. P. J. Albracht and W. Lubitz, *J. Biol. Inorg. Chem.*, 2007, **12**, 212-233.
36. B. L. Greene, C. H. Wu, P. M. McTernan, M. W. Adams and R. B. Dyer, *J. Am. Chem. Soc.*, 2015, **137**, 4558-4566.
37. J. O. Alben, P. P. Moh, F. G. Fiamingo and R. A. Altschuld, *Proc. Natl. Acad. Sci. U. S. A.*, 1981, **78**, 234-237.
38. K. A. Vincent, A. Parkin and F. A. Armstrong, *Chem. Rev.*, 2007, **107**, 4366-4413.
39. B. Bleijlevens, F. A. Broekhuizen, A. L. De Lacey, W. Roseboom, V. M. Fernandez and S. P. J. Albracht, *J. Biol. Inorg. Chem.*, 2004, **9**, 743-752.
40. P. A. Ash, R. Hidalgo and K. A. Vincent, *ACS Catal.*, 2017, **7**, 2471-2485.
41. T. Watanabe and K. Honda, *J. Phys. Chem.*, 1982, **86**, 2617-2619.

42. Y. Takayama, C. A. Castañeda, M. Chimenti, B. García-Moreno and J. Iwahara, *J. Am. Chem. Soc.*, 2008, **130**, 6714-6715.
43. A. Pardo, A. L. Lacey, V. M. Fernandez, H.-J. Fan, Y. Fan and M. B. Hall, *J. Biol. Inorg. Chem.*, 2006, **11**, 286-306.
44. A. Volbeda, E. Garcin, C. Piras, A. L. de Lacey, V. M. Fernandez, E. C. Hatchikian, M. Frey and J. C. Fontecilla-Camps, *J. Am. Chem. Soc.*, 1996, **118**, 12989-12996.
45. C. Fichtner, C. Laurich, E. Bothe and W. Lubitz, *Biochemistry*, 2006, **45**, 9706-9716.
46. M.-E. Pandelia, P. Infossi, M. T. Giudici-Ortoni and W. Lubitz, *Biochemistry*, 2010, **49**, 8873-8881.
47. A. L. De Lacey and V. M. Fernandez, *Chem. Rev.*, 2007, **107**, 4304-4330.
48. A. L. DeLacey, C. Stadler, V. M. Fernandez, E. C. Hatchikian, H.-J. Fan, S. Li and M. B. Hall, *J. Biol. Inorg. Chem.*, 2002, **7**, 318-326.
49. K. A. Bagley, C. J. Van Garderen, M. Chen, W. H. Woodruff, E. C. Duin and S. P. J. Albracht, *Biochemistry*, 1994, **33**, 9229-9236.
50. Y. Ilina, C. Lorent, S. Katz, J.-H. Jeoung, S. Shima, M. Horch, I. Zebger and H. Dobbek, *Angew. Chem., Int. Ed.*, 2019, **58**, 18710-18714.
51. M.-E. Pandelia, H. Ogata, L. J. Currell, M. Flores and W. Lubitz, *Biochim. Biophys. Acta, Bioenerg.*, 2010, **1797**, 304-313.